On Drive Systems for High Performance Machines
And
Design of an Air Motor/Particle Brake Actuator

by

Kenneth Alan Pasch

BSME, Massachusetts Institute of Technology
(1981)

SUBMITTED TO THE DEPARTMENT OF
MECHANICAL ENGINEERING IN
PARTIAL FULFILLMENT OF TnE
REQUIREMENTS FOR THE DEGREE OF

MASTER OF SCIENCE IN
MECHANICAL ENGINEERING

at the

MASSACHUSETTS INSTITUTE OF TECHNOLOGY

April 1984

© Massachusetts Institute of Technology 1984

Signature of Author _____
Department of Mechanical Engineering
April 1984

Certified by_ _____
Warren Paul Seering
Thesis Supervisor

Accepted by _____
Warren Max Rohsenow
Chairman, Departmental Graduate Committee

On Drive Systems for High Performance Machines
And
Design of an Air Motor/Particle Brake Actuator

by

KENNETH ALAN PASCH

Abstract

Methods are presented for choosing actuators and transmission elements for one-degree-of-freedom machines. Cases considered are choice of actuator and transmission ratio for maximum system acceleration given generalized impedance at the actuator and the load, and optimal transmission ratio selection for a velocity limited incremental motion system. General torque, angular velocity, power consumption and power dissipation for a system with given velocity and acceleration specifications are described.

Application of these methods illustrates the value of an alternative high performance actuator, which is the combination of a solenoid-valve-controlled rotary-vane-type air motor and a servoable magnetic particle brake. Theory of operation of this device is developed, and a digital closed-loop position-control scheme is implemented. The controller was designed by constraining the system not to reverse velocity during step response while minimizing the integral time absolute error.

Device performance was simulated and a prototype designed, constructed and tested. Results show that it is possible to servo such a device; however, some components must be redesigned in order to realize the full potential of the actuator.

Thesis Supervisor: Warren Paul Seering

Title: Assistant Professor of Mechanical Engineering

Acknowledgments

Table of Contents

1. Introduction to Actuator and Transmission Choice

Recently, the importance of the design of high performance machines and particularly of robotic manipulators has been widely acknowledged [1]. However relatively little work has been done on the choice and design of the mechanical components for the best dynamic performance. Various authors have evaluated manipulator kinematic performance and have set guidelines for configuration of manipulator links and joints [2,3]. Others [4,5] have developed algorithms for defining the boundaries of the workspace for manipulators with arbitrarily complex kinematic configurations. A thorough study of the state of the art in the computer control of robot manipulators has been presented by Paul [6]. A number of authors have studied methods for enhancing manipulator performance using special control algorithms [7]. Hollerbach [8] has developed an efficient analytical formulation of manipulator dynamics for use in real time control. Methods for feedback control of flexible link manipulators have been presented by Book [9] and Book et al. [10]. Sunada and Dubowsky [11] have developed methods for the analysis of industrial manipulators with complex shaped flexible links. They have concluded that link and joint flexibility can have significant impact on system performance and stability.

Methods are presented for choosing actuators and transmission elements for one-degree-of-freedom machines. Cases considered are choice of actuator and transmission ratio for maximum system acceleration given generalized impedance at the actuator and the load, and optimal transmission ratio selection for a velocity limited incremental motion system. General torque, angular velocity, power consumption and power dissipation for a system with given velocity and acceleration specifications are described.

Application of these methods illustrates the value of an alternative high performance actuator which is the combination of a solenoid-valve-controlled rotary-vane-type

air motor and a servoable magnetic particle brake. Theory of operation of this device is developed, and a digital closed-loop position-control scheme is implemented. The controller was designed by constraining the system not to reverse velocity during step response while minimizing the integral time absolute error.

Device performance was simulated and a prototype designed, constructed and tested.

2. Methods for Choosing Actuators

Max Acceleration for a Given Amplitude of Actuator Effort

Proper choice of system transmission ratio is necessary to produce maximum system acceleration. A typical one degree-of-freedom mechanical system consists of a torque or force source, a transmission, and an inertial load. One such system, a DC motor-ball screw system is presented schematically in Figure 1. In general, the inertial load, M, can represent a mass as in a prismatic joint or a rotary inertia as in a rotating element. For systems with varying geometry, such as the $PUMA^{TM}$ robot, rotary inertia about a given joint varies as a function of system orientation. Such systems should be designed to give maximum acceleration at a position near the center of the workspace. For the model of Figure 1, the torque source is assumed to have a rotary inertia J and to produce a torque T. The transmission ratio, r, is defined as the ratio of transmission output velocity to input velocity. For a gear transmission system, r is the ratio of output angular velocity to input angular velocity. For the case of a ball screw system, r is the ratio of output translational velocity to input angular velocity in rad/s. For a rack and pinion system, r is also the ratio of the output translational velocity to the input angular velocity and is equal in magnitude to the radius of the pinion pitch circle.

For many high performance applications, it is desirable to maximize system output acceleration, a. The equation of motion for the system in Figure 1 is

$$T = (\frac{J}{r} + Mr)a \qquad (1)$$

A value can be found for r which minimizes the quantity in brackets, thus maximizing acceleration for a given actuator effort.

$$\frac{\partial(J/r + Mr)}{\partial r} = \frac{-J}{r^2} + M = 0$$

Figure 1. Model of a Servo System

Figure 1. Model of a Servo System
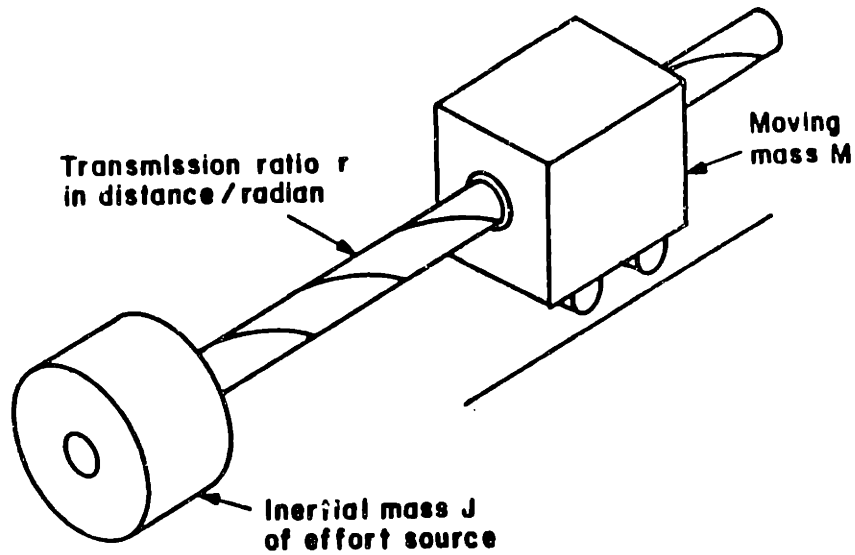
or

$$r' = \sqrt{\frac{J}{M}} \tag{2}$$

In this equation, r' is the transmission ratio which will yield the greatest system acceleration for a given actuator effort. Note that substitution of r' for r in Eq. (1) produces equal 'impedance' contributions for the rotary inertia and the moving mass. This choice of r then gives an 'impedance matched' system. Figure 2 is a plot of a^* versus r^*. The terms a^* and r^* are dimensionless parameters defined as

$$r^* = \frac{r}{r'} \tag{3}$$

8

Figure 2. Achievable System Acceleration as a Function of Lead Choice
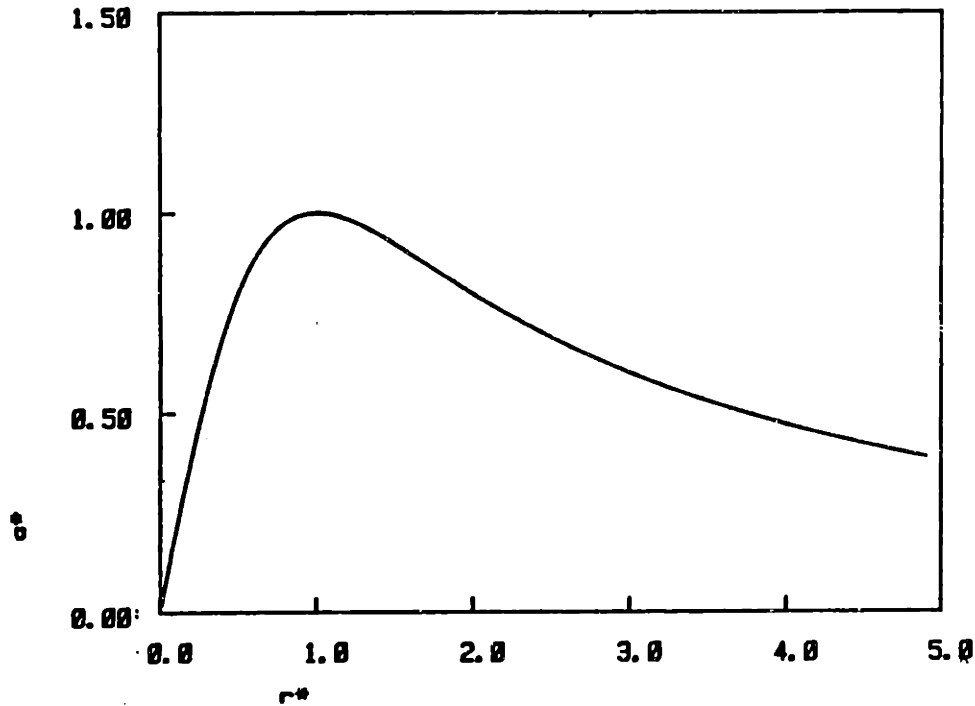
$$a^* = \frac{a}{a_{max}} \qquad (4)$$

where from Eq. (1) with $r = r'$

$$a_{max} = \frac{T/\sqrt{J}}{2\sqrt{M}} \qquad (5)$$

In Figure 2, a^* is seen to be insensitive to small changes in r^* near $r = r'$. However a^* decreases markedly with larger decreases in r^*. From Eq. (5), peak system acceleration a_{max} is seen to be proportional to $T/\sqrt{J}$. Hence, assuming optimal lead selection, for a bigger motor to yield a greater acceleration, percent increase in torque must be greater than percent increase in $\sqrt{J}$.

Many systems, such as DC servo motors with current amplifiers, can produce constant torque output regardless of angular velocity. For other systems, torque

is a function of angular velocity w. In these latter cases, the transmission ratio calculated above [Eq. (2)] will give maximum achievable acceleration at all values of w. Peak acceleration will of course occur at the value of w for which T is greatest.

Motor Selection For Maximum Acceleration

Equation (5) quantifies the dependence of system acceleration on system torque and inertia. Assume for the moment that J_s, the inertia of the transmission element, is small as compared with J_m, the inertia of the motor. Equation (5) can be rewritten

$$\frac{T}{\sqrt{J_m}} \sim 2a_{max}\sqrt{M} \tag{6}$$

for the case in which the optimal lead has been chosen.

In Figure 3 are plotted values of rotor inertia versus motor torque for several families of motors ranging in size (and cost) over two orders of magnitude. Values for T and J_m were obtained from manufacturers catalogs. From Eq. (6), lines of constant $a_{max}\sqrt{M}$ can be plotted on the figure. If the moving mass of the system is known, the system acceleration produced by each of the motors can be read directly from the chart. For Figure 3, a moving mass of 50 lbm (23 kg) was chosen and constant acceleration lines were plotted for accelerations up to 5g.

The plot in Figure 3 reveals that for most families of motors, larger and more expensive motors do not produce significantly greater acceleration. In fact for brushless motors, the largest motor included produces the lowest acceleration. There is however an advantage to using larger motors. Because they have larger values of J, larger values of r' [see Eq. (2)] will be chosen for maximum acceleration. And for a larger chosen value of r', the peak velocity of the moving mass will be larger for a given peak motor angular velocity.

Once a transmission element for a system has been chosen and its rotary

Figure 3. Motor Performance for Various Families of Motors in Systems with Optimized Lead
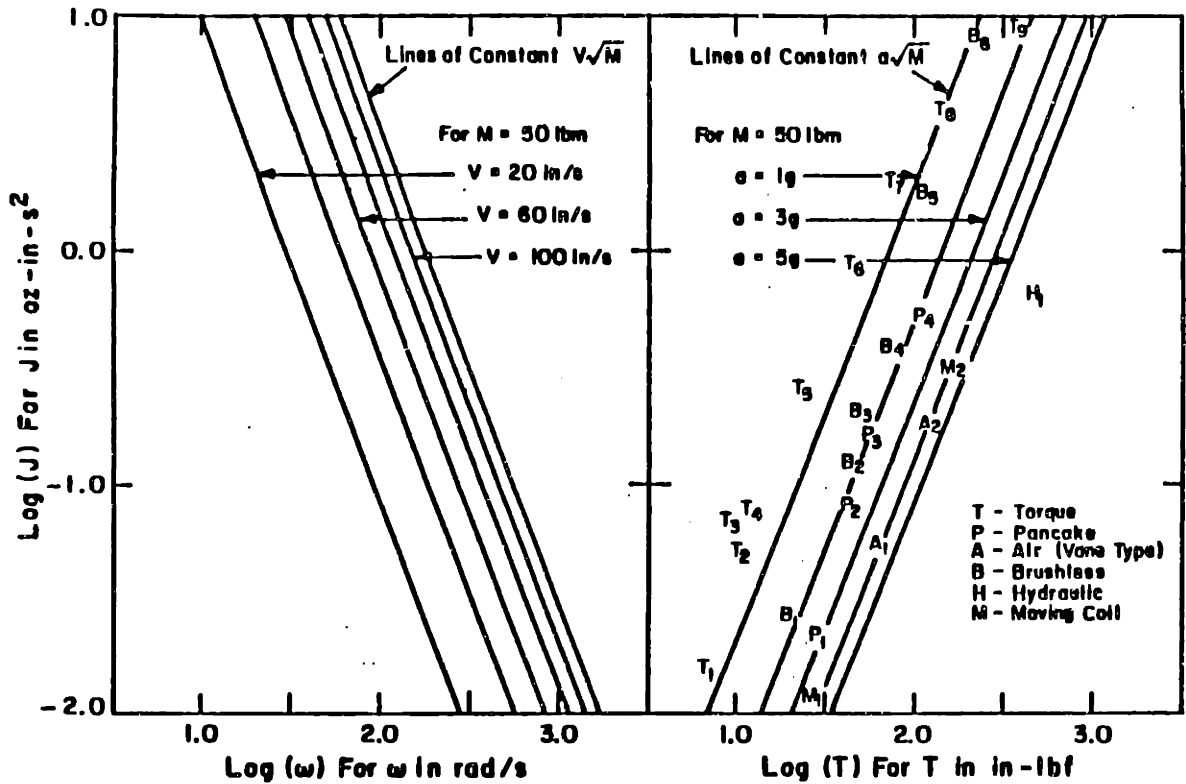
inertia J_s determined, a corrected value for system acceleration can be obtained from Figure 3. The addition of the inertia J_s simply shifts the location of the point representing the chosen motor to the right to account for the fact that the abscissa J is now taken to represent the sum of the inertias J_s and J_m. For a given value of J_s, system performance will be affected less for larger values of J_m.

Correction of the value of J by inclusion of J_s will increase the value of r'. In certain cases, this change in r', because of limitations on transmission element design, will necessitate a change in dimension of a transmission element resulting in an increase in J_s. When this occurs, an iteration process must be employed to establish optimal choices of J_s and r'. It should be noted however that for

transmission elements such as ball screws, transmission ratios r' are only available in discrete increments. This is not a serious disadvantage as from Figure 2 we again note that system performance is relatively insensitive to small variations in r about the optimal value $r = r'$.

On the left side of Figure 3 are plotted lines of constant $V_{max}\sqrt{M}$ assuming optimal lead choice where V_{max} is the peak speed of the driven mass. From system geometry

$$V_{max} = r'w_{max} = w_{max}\sqrt{\frac{J}{M}}$$

or

$$V_{max}\sqrt{M} = w_{max}\sqrt{J} \qquad (7)$$

Values for w_{max} in a given system may be dictated by motor manufacturer's data or by other system considerations such as resonant excitation of the drive system. Having chosen a motor and transmission and having determined the value of w_{max}, one can find from the left side of Figure 3 the peak velocity of the moving mass. This plot illustrates that at a given w_{max}, for motors producing a given acceleration, those with greater values of J will produce greater peak velocities of the driven mass. This is particularly important if the system will spend a significant amount of time operating at peak velocity. Design of such systems will be discussed later.

Effects of Changes in Rotary Inertia on System Performance

As discussed in the previous section, inclusion of transmission inertia J_s decreases predicted system peak acceleration. This effect, however, is small in most cases because transmission inertia is usually small as compared to motor inertia. For a given system, from equations(2) and (3), r^* can be calculated as

$$r^{\bullet} = \frac{r\sqrt{M}}{\sqrt{J_m + J_s}} \qquad (8)$$

Consider now the system acceleration. From equation(5)

$$a_{max} = \frac{T}{2\sqrt{(J_s + J_m)M}}$$

Rearranging

$$\frac{2a_{max}\sqrt{MJ_m}}{T} = \frac{1}{\sqrt{1 + J_s/J_m}} \qquad (9)$$

This equation is presented graphically in Figure 4 to illustrate the effect of increasing transmission inertia on the system acceleration. As would be expected, the best one can do is the limiting case of zero transmission inertia. One example of this would be rack and pinion drive where the pinion inertia in neglible in comparison to the motor inertia.

Effects Of Changes In Driven Mass On System Performance

Let $M = M_c + M_p$, the sum of the fixed and payload masses. Figure 5 shows the effect on system performance of changes in M_p over a range of values of the transmission ratio $r^{\bullet}$. Also plotted is a line of peak acceleration for variations in M_p/M_c. This plot illustrates that optimal value for the transmission ratio does not vary significantly through a range of small values for M_p/M_c. This is fortunate as the transmission ratio for most systems is difficult to change during operation. Figure 5 also shows that for values of $r^{\bullet}$ less than 0.4, system acceleration at a given torque is virtually independent of M_p/M_c. This fact has lead many system designers to choose low values of $r^{\bullet}$ to simplify the problem of system control. As can be seen from the figure, this choice imposes a substantial performance penalty.

Figure 4. Change in Achievable System Acceleration
with Increase in Transmission Inertia J_s
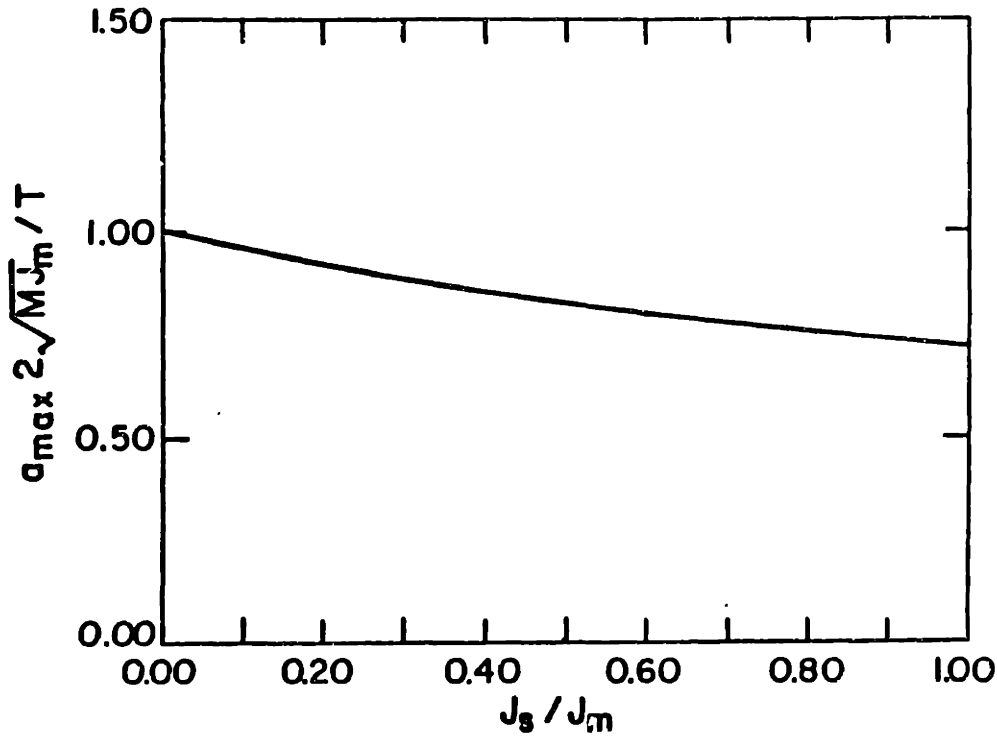
Effects of Generalized Impedance at Load and Source

We now consider the case where the load is a generalized impedance which has inertial, viscous drag, and static force components both at the motor and at the moving mass.

The equation of motion for such systems is

$$a = [(T - r) - (\frac{b}{r} + Br)V - Fr]/(\frac{J}{r} + Mr) \tag{10}$$

where r, b, and J are static, viscous, and inertial loads at the motor; F, B, and M are corresponding loads at the moving mass; and V is a chosen system mass velocity. Maximizing acceleration with respect to r at the chosen velocity V and expressing the result in terms of r^* gives

14

Figure 5. Effect on System Performance of Increase in Moving Mass
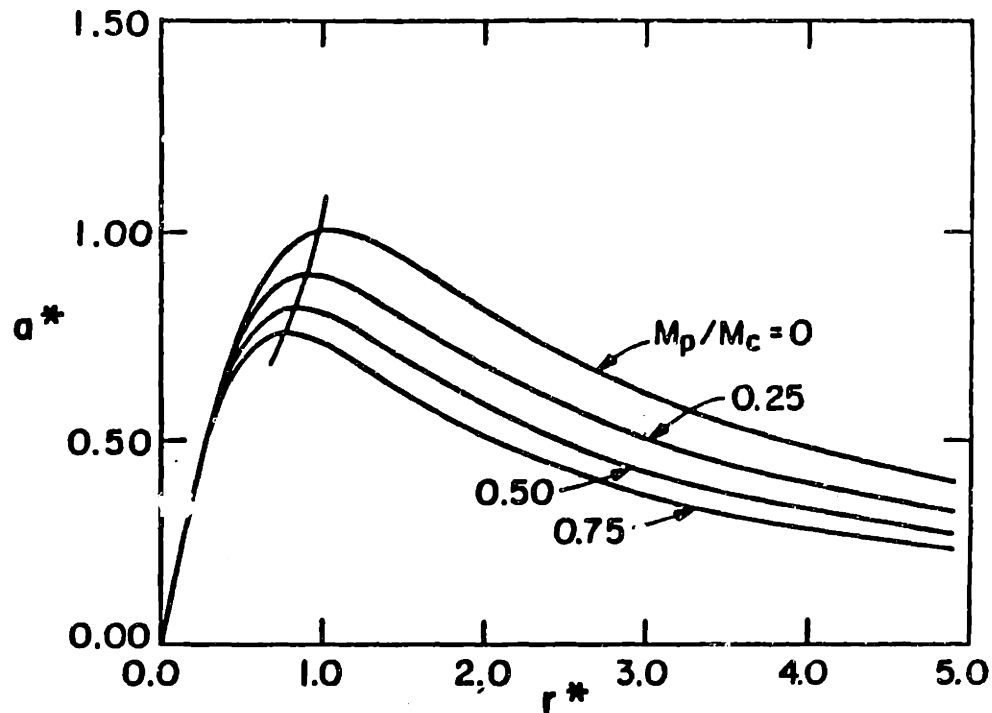
$$(r^*)^2 + 2r^*\Delta - 1 = 0 \tag{11}$$

$$\Delta = [(BV + F)\sqrt{\frac{J}{M}} - bV\sqrt{\frac{M}{J}}]/(T - \tau) \tag{12}$$

Solving this quadratic and discarding the negative root yields

$$\Gamma = \sqrt{1 - \Delta^2} - \Delta \tag{13}$$

where Γ is the optimal value of r^* for a system with losses. To help visualize the contributions of the various disturbances, equation (10) can be rewritten as follows:

$$a = (T - \tau)/(\frac{J}{r} + Mr) - (F + BV)r/(\frac{J}{r} + Mr) - (bV/r)/(\frac{J}{r} + Mr)$$

or

$$a^* = 2(1 - \overline{A} - \overline{B}r^* - \overline{C}/r^*)/(r^* + 1/r^*) \tag{14}$$

where

$$\overline{A} = \tau/T$$

$$\overline{B} = (F + BV)\sqrt{\frac{J}{M}}/T$$

$$\overline{C} = bV/(T\sqrt{\frac{J}{M}})$$

As defined here, $\overline{A}$ is a measure of static resistive load at the effort source, $\overline{B}$ is a measure of impedance at the driven mass, and $\overline{C}$ is a measure of viscous load at the effort source. The four curves in Figure 6 correspond to the cases

Case	$\overline{A}$	$\overline{B}$	$\overline{C}$
1	0	0	0
2	0.15	0	0
3	0	0.15	0
4	0	0	0.15

Notice that the different types of disturbances have the same net effect of lowering the peak acceleration while the value of the optimum transmission ratio shifts in different directions with inclusion of different types of impedance. However,

Figure 6. Effect on System Performance of Various Types of Loads
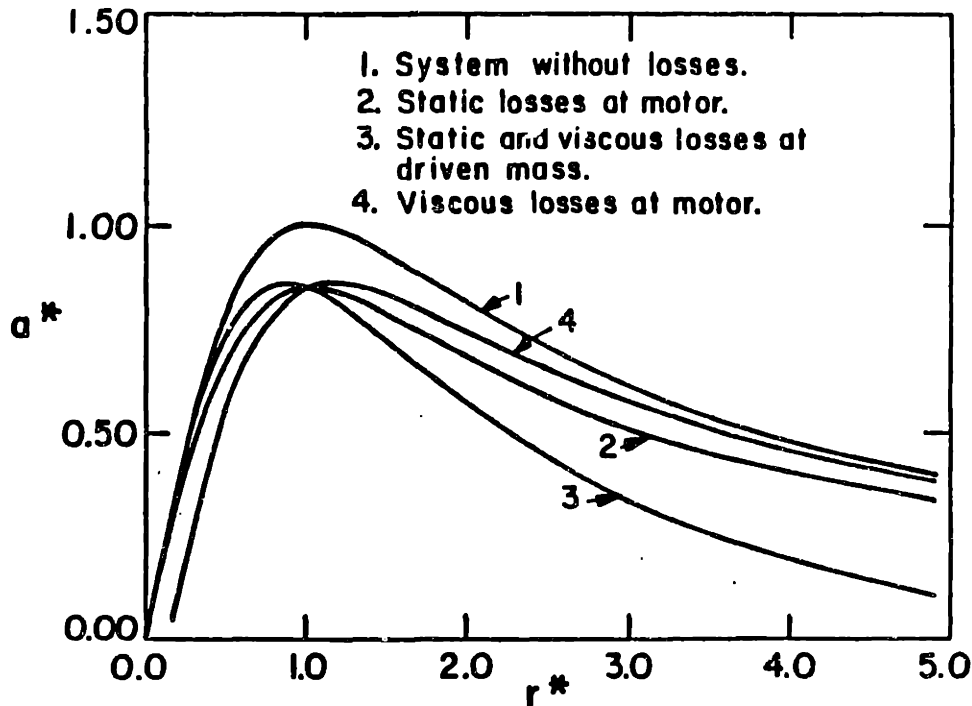
for each case shown, choice of $r^* = 1$ as the system transmission ratio results in small degradation in performance as compared with that for the best possible lead choice.

Figure 6 represents a system operating at a velocity V. Results in cases 1 and 2 are independent of choice of V. The curves for cases 3 and 4 will shift as the chosen velocity V changes, but if the system viscous damping coefficients are small, the shifts of these curves with V will also be small.

Torque, Angular Velocity, Power Consumed, and Power Dissipated

Other system considerations besides maximization of acceleration suggest r' as the optimal system transmission ratio. For a system with driven mass traveling at a chosen velocity V_{spec} and accelerating at a specified rate, A_{spec}, define w_m to be V_{spec}/r'. Then the dimensionless ratio w^* can be defined as

$$w^\bullet = \frac{w}{w_m}$$

for any w. Next define T_m as the torque required to produce a_{spec} with the transmission ratio r'.

$$T_m = 2a_{spec}\sqrt{JM}$$

The dimensionless ratio $T^\bullet$ can be defined as

$$T^\bullet = \frac{T}{T_m} \tag{17}$$

Power required to produce acceleration a_{spec} at velocity V_{spec} is

$$Hp = Tw$$

The dimensionless quantity $Hp^\bullet$ is defined as

$$Hp^\bullet = \frac{Tw}{T_m w_m} = T^\bullet w^\bullet \tag{18}$$

For the case of a d-c motor as an effort source, power dissipated through ohmic heating of the motor is $P = I^2 R$ where to a first approximation I, the motor current, equals T/k with k the motor torque constant. For $a = a_{spec}$ and $V = V_{spec}$, and for $r = r'$, power dissipated is

$$P_m = R(\frac{T_m}{k})^2$$

Although only a small fraction of the power going into the motor is dissipated by ohmic heating, it has a substantial effect on the motor operating temperature.

All dissipated power must be conducted to the environment and the path is usually across the rotor/stator air gap and through the rotor shaft and bearings. In this analysis, windage, hysteresis, and frictional heating have been neglected as they are not a problem in general. From the previous equation, P^*, a dimensionless ratio of dissipated power, can be defined as

$$P^* = \frac{R(T/k)^2}{R(T_m/k)^2} = (T^*)^2 \tag{19}$$

Figure 7 displays these system characteristics over a range of values of r^* with a and V specified. At $r^* = 1$, T^* is minimized. For r less than r' the inertial loading of the motor dominates system impedance and for r greater than r' the inertial loading of the driven mass dominates. Because power dissipated is proportional to T^2, ohmic heating is also minimized at $r^* = 1$.

In the limit as r^* approaches infinity, power consumed goes to MaV. This is the power required to meet the specs if motor inertia is taken to be zero. At $r^* = 1$, power consumed is $2MaV$. In this case, power accelerating the mass equals power accelerating the motor inertia.

Motor Selection For A Given System

Many times, the design engineer cannot specify all system parameters. Rather, the task may be to specify a motor to drive an existing system. In this case J_s, r, and M are known, and the governing system equation can be written

$$T = ac_1 J_m + ac_2 \tag{20}$$

where

$$c_1 = \frac{1}{r}$$

**Figure 7. Effect of Transmission Ratio on Motor
Requirements for a Given Performance Level**
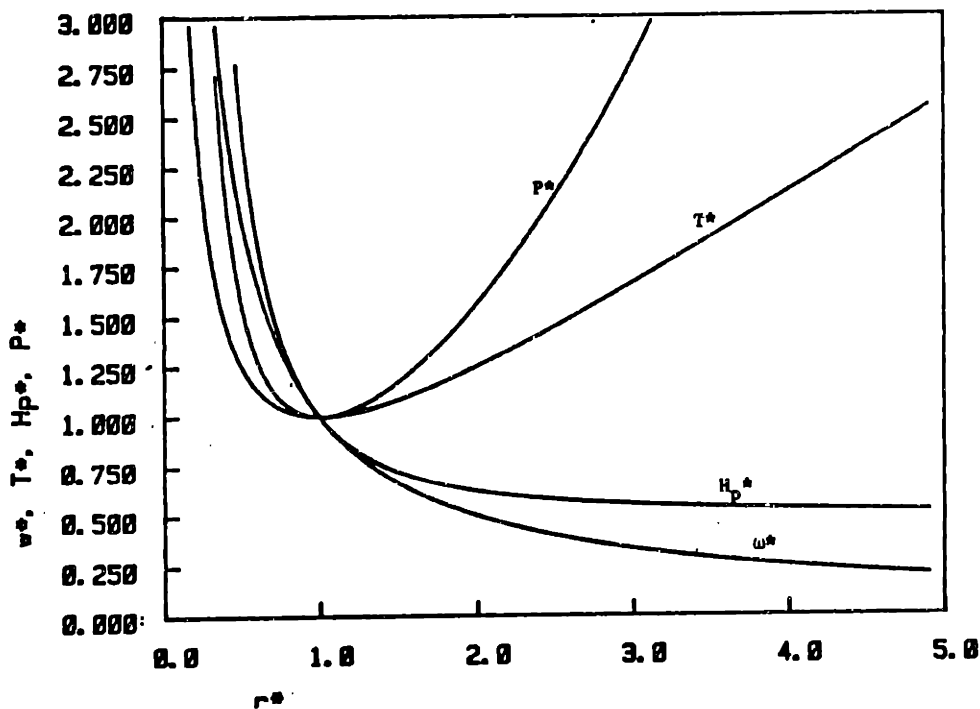
$$c_2 = \frac{J_s}{r} + Mr$$

This equation shows torque required to produce a given acceleration to be a linear function of motor inertia.

Figure 8 gives constant acceleration lines on a plot of torque versus motor inertia. As can be seen from Eq. (7), for a motor change to produce greater acceleration of the translating mass, increase in torque must be greater than (a/r) times the increase in J_m. Hence, as indicated in Figure 8, the greater the initial value of a, the greater must be the change in T for a given change in J_m if system acceleration is to be increased.

Figure 8. Performance Curves for Motors in Systems with Fixed Transmission Ratios
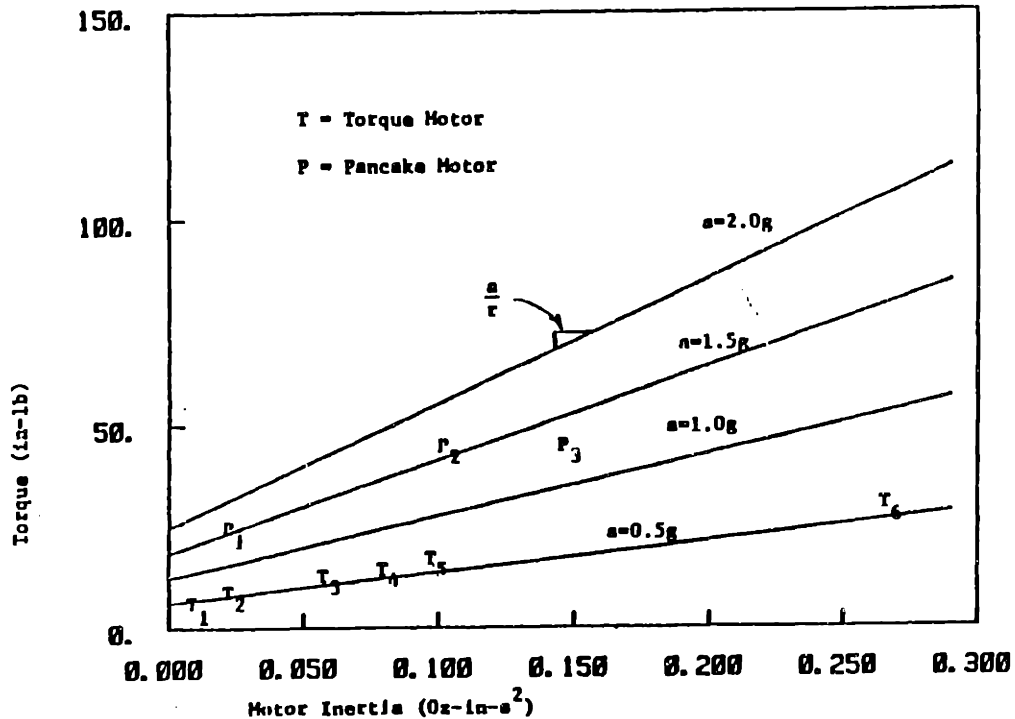
Determining Optimal Lead For Velocity Limited Systems

Maximizing acceleration does not guarantee that a system will be time optimal for all moves. Top speed (rw_{max}) may be reached in the minimum time but choice of transmission ratio might unnecessarily limit this top speed for a given allowable peak motor or transmission angular velocity.

Consider the velocity profile for one of the incremental moves shown in Figure 9. This move could be produced by a DC servo motor which has constant torque but is speed limited to top speed w_{max}. Note that for $r = r'$ the slopes at the beginning and end of the move are steepest. The area under the curve represents the distance traveled during the move. For the case in which the system does not dwell at peak velocity, the transmission ratio which minimizes total move time is

Figure 9. Typical Incremental Move Velocity Profiles
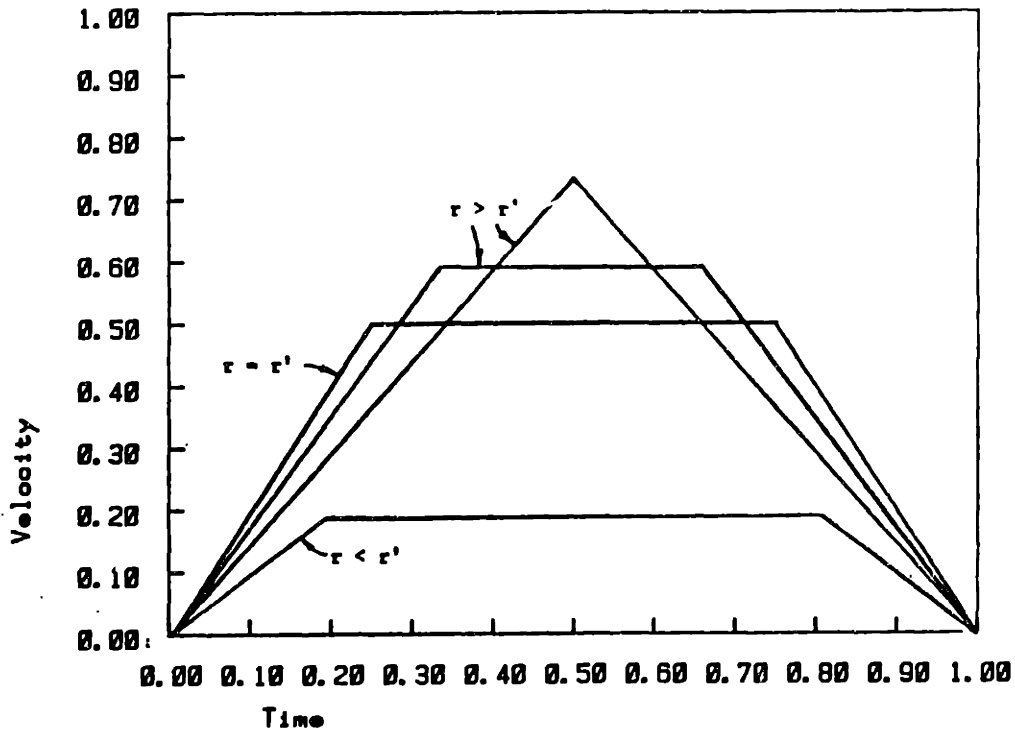
$r = r'$. If the system dwells at top speed, $r = r'$ is no longer the optimal ratio. Notice that for r less than r', the slope of the velocity versus time line is decreased as is the top speed. Thus as r decreases from r', the area under the curve will always decrease for a move of fixed time duration. For r slightly larger than r' the area under the curve increases with r. At some value of increasing r, the area starts to decrease.

For a typical move in which the system reaches peak velocity it can be shown that travel time t_t is

$$t_t = \frac{w_{max}(J + Mr^2)}{T} + \frac{d}{rw_{max}} \qquad (21)$$

where d is the total move distance. Taking the partial derivative of this equation with respect to transmission ratio gives

$$\frac{\partial t_t}{\partial r} = 0 = \frac{(2rMw_{max})}{T} - \frac{d}{w_{max}r^2}$$

or

$$r_{opt} = \left(\frac{Td}{2Mw_{max}^2}\right)^{1/3} \tag{22}$$

where r_{opt} is the transmission ratio which minimizes time required to perform a specified move, d, for the case in which the system dwells at $w = w_{max}$.

It can be shown that if a constant torque system with transmission ratio r' accelerates until $w = w_{max}$ and then immediately decelerates to a stop, distance traveled is

$$d_m = \frac{2w_{max}^2 J^{3/2}}{T\sqrt{M}} \tag{23}$$

Define a dimensionless parameter d^* as

$$d^* = \frac{d}{d_m} \tag{24}$$

Where d is the distance traversed in an incremental move. Then from equations(21),(22), and (23),

$$\begin{aligned} r_{opt} &= (d^*)^{1/3} && \text{if } d^* \geq 1 \\ r_{opt} &= 1 && \text{if } d^* < 1 \end{aligned}$$

This relationship is plotted in figure 10.

Generally, machines under computer control do not have a fixed move distance. Rather, they move through a range of distances. Figure 11 illustrates the effect on time required to move a given distance of choice of transmission ratio for systems

Figure 10. Optimal Lead Versus Move Distance
for Incremental Motion Systems
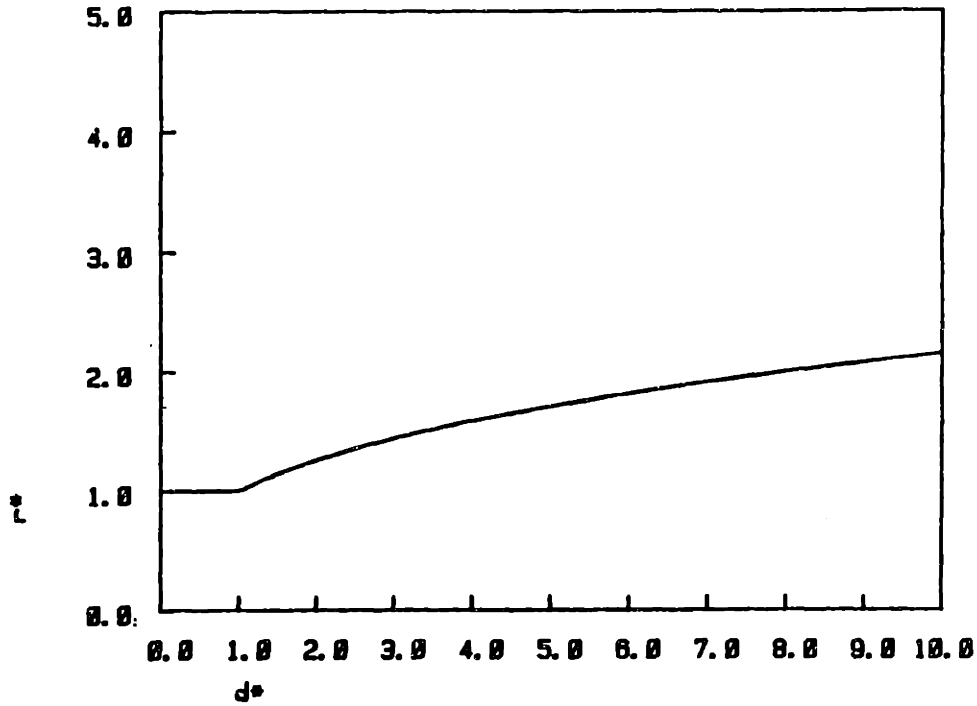
which may reach peak speed. The transmission ratio of choice in the figure would be the one which does the best job of minimizing t^* throughout the range of interest of d^*. For this plot dimensionless time t^* is defined as

$$t^* = \frac{t}{Jw_{max}/T} \tag{26}$$

where Jw_{max}/T is time required for the system to reach w_{max} for the case of $M = 0$.

From equations(21) and (22), time for a move of distance d is

$$t_t = \frac{Jw_{max}}{T} + 3(\frac{Md^2}{4Tw_{max}})^{1/3} \tag{27}$$

Figure 11. Move Distance Versus Time for Various Transmission Ratios
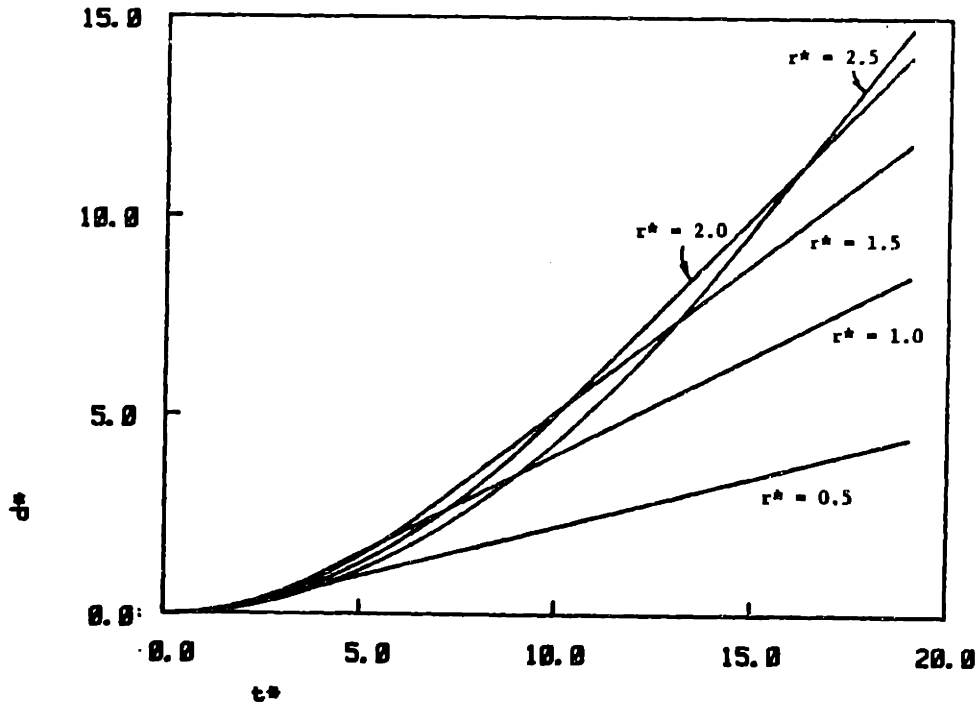
which can be rewritten

$$\frac{Jw_{max}}{T} = t_t - 3(\frac{Md^2}{4})^{1/3}(\frac{1}{Tw_{max}})^{1/3}$$

Figure 12 is a plot of motor parameters Jw_{max}/T (in units of time) versus $1/(Tw_{max})^{1/3}$. As in Fig 3, motors from a range of motor families can be placed on the plot according to values obtained from catalogues or possibly (for w_{max}) from other system considerations. From this equation it can be seen that the time required for a system with $r = r_{opt}$ to move a distance d is the ordinate intercept of a line in Fig 12 through the point representing the system motor and having a slope of $-3(Md^2/4)^{1/3}$. If M and d are known, one can determine required move time, t_t, for any of the motors plotted. Motors appearing near the origin will tend to require less time to produce a given move. They will also tend to cost more.

25

Figure 12. Motor Performance for Various Motors in Velocity Limited Systems
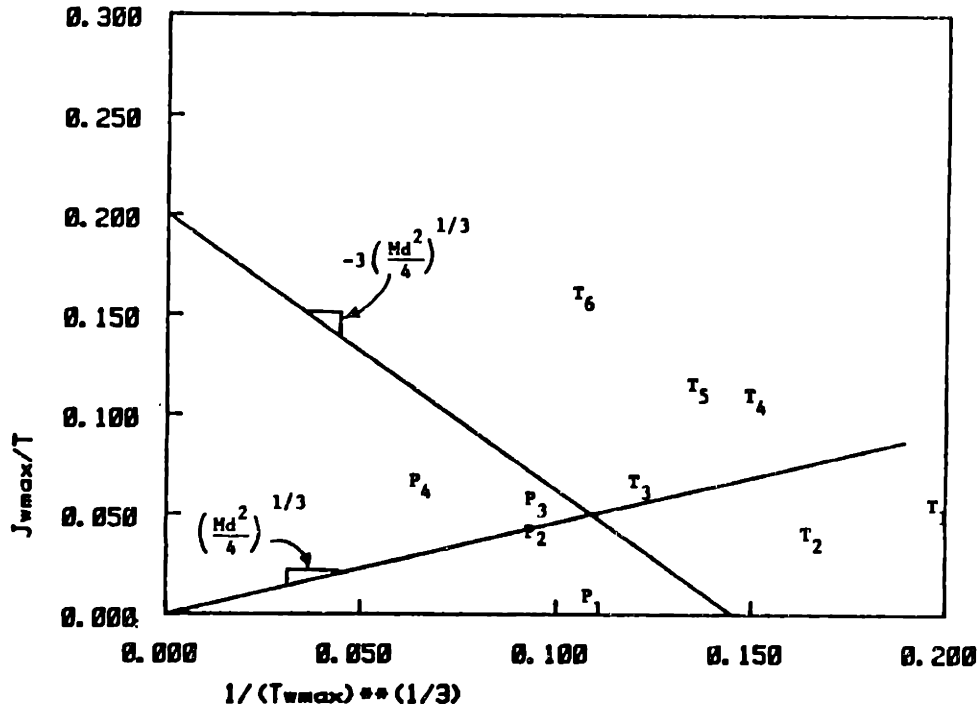
This figure is valid only for $d^* \geq 1$. A region on the plot for which d^* is less than 1 is below a line passing through the origin and having a slope of $(d^2 M/4)^{1/3}$. Motors within this region will not reach peak speed during a move of distance d.

Summary of Actuator and Transmission Choice

To extract the greatest possible performance from a mechanical system, one must make a judicious choice of system parameters. In the absence of dissipative forces, the transmission ratio $r = \sqrt{J/M}$ will give maximum acceleration for many systems. Introduction of dissipative forces will reduce peak acceleration but will not substantially change the value of the optimal transmission ratio. Introduction of additional masses at the moving endpoint mass will not significantly change the optimal transmission ratio either. If system transmission ratio is set without knowledge of other system parameters, it is unlikely that optimal performance will

be achieved.

Choice of transmission ratio is somewhat more complex for the case in which the peak operating speed of a system is reached. Minimum time for a given move is obtained when the transmission ratio, r, equals $(Td/(2Mw_{max}^2))^{1/3}$. This expression suggests that for wide ranges of move distance, variation in optimal transmission ratio is small.

3. Design of the Actuator

3.1. About Air Motors

As can be seen in figure (3) the air motor has a very high torque to square-root-of-inertia ratio. While this feature is attractive, the inherent compliance of air as part of a servo system poses bandwidth limitations (the fastest a signal can travel along a pneumatic circuit is MACH 1, which is slow relative to the propagation of electrical signals)

As an alternative to modulation of the air motor input, it is proposed to use the air motor to only supply torque to the system which is then modulated using a servoable braking device. A magnetic particle brake was chosen for this task as it has an extremely high (much higher than DC or hydraulic motors) torque to square-root-of-inertia ratio. This device is also easily interfaced to electronic control hardware.

Theoretically, this hybrid actuator will be capable of producing higher accelerations than DC servo motors including those of the samarium cobalt and pancake types. This is surprising given the fact that air motors are not designed (at least not the vane type) for high accelerations. A typical vane motor rotor might consist of a solid cast iron rotor with a few slots milled radially to accommodate sliding vanes.

Unfortunately, air power is more expensive than power obtained through direct electrical to mechanical conversion. To start out, the electric energy is transduced to mechanical energy and stored in a compressed gas. From there it is transduced back to mechanical power. Since no transduction process is 100% efficient, energy is lost at each step. The process efficiencies vary depending upon device and operation conditions. For example, an electric motor may have a 90% efficiency (power out/power in) when operating under its most favorable conditions, however

this approaches zero as the motor approaches the stall; where the motor generates heat instead of useful work. In comparison, a rotary vane type air motor may have a maximum efficiency of 40% under it's most favorable operating conditions, but does not undergo such a radical change in efficiency as the motor approaches stall because power consumed also approaches zero (little or no air flows through the motor at stall).

It is expected that the relatively slow propagation of pneumatic signals, entrained air, and solenoid valve switch time will limit overall system bandwidth, especially when switching directions. Another problem associated with air motors is that they require oil mist lubrication which contaminates the ambient air.

3.2. Motor Model and Characteristics

The air motor used does not have linear torque speed characteristics. Rather, it has those shown in Figure 13. Notice that the slope of the curve changes by one order of magnitude and in sign when passing through the $300RPM$ point. This means that a feedback coefficient in a minor loop is going to change by one order of magnitude and in sign.

The size of the air motor for the design prototype was determined by the drive requirements for the largest axis of the MIT Cartesian Assembly Robot. The axis specifications were; weight $60lbs$, acceleration 2-$3g's$, and top speed $2m/s$. The motor selection curves of Figure 3 illustrate that the Gast rotary vane motor is sufficient for the task. This is a standard $1.5hp$, $300 item. To control the air flow to the motor, a Norgren 4-way, $3/8in$ npt port size, solenoid valve was chosen. This valve has approximately a $16ms$ switch time.

3.3. Brake Characteristics

The brake used in the hybrid actuator is not an ideal torque sink. The torque current curves for the device are shown in Figure 14. Notice that in addition to

Figure 13. Actual Air Motor Torque/Speed Curves

Torque vs. RPM of Gast model 4AM air motor
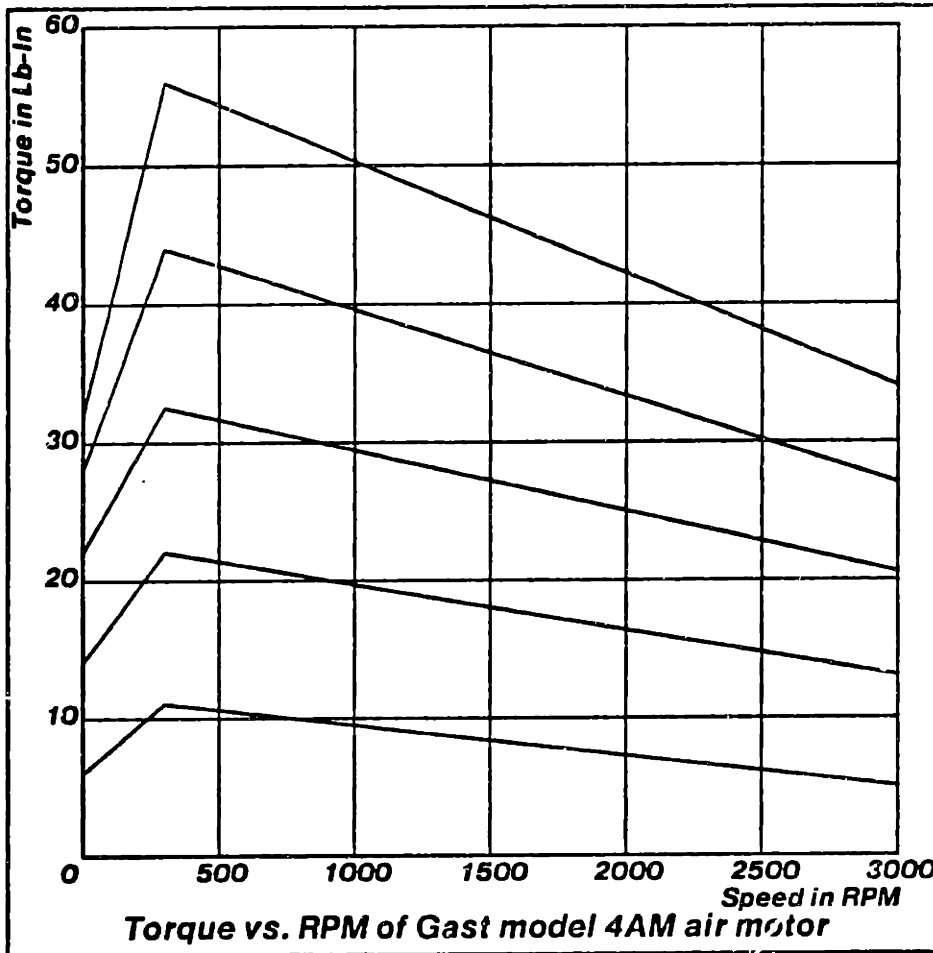
indicating magnetic saturation (decreasing rate of change of torque with increasing current), the curves also show a large amount of hysteresis.

The particle brake was specified to have enough torque to completely overpower the air motor. This was so that one could start and stop the device in one direction without having to switch the air pressure off in order to stop. The maximum brake torque is approximately 3 times the peak motor torque. This high brake torque should allow for higher deceleration than acceleration, especially if the motor torque is reversed while the device is still traveling forward. Another reason for this high torque is for holding position once a destination is reached. The brake used here is a

Figure 14. Actual Torque/Current Curves for Particle Brake
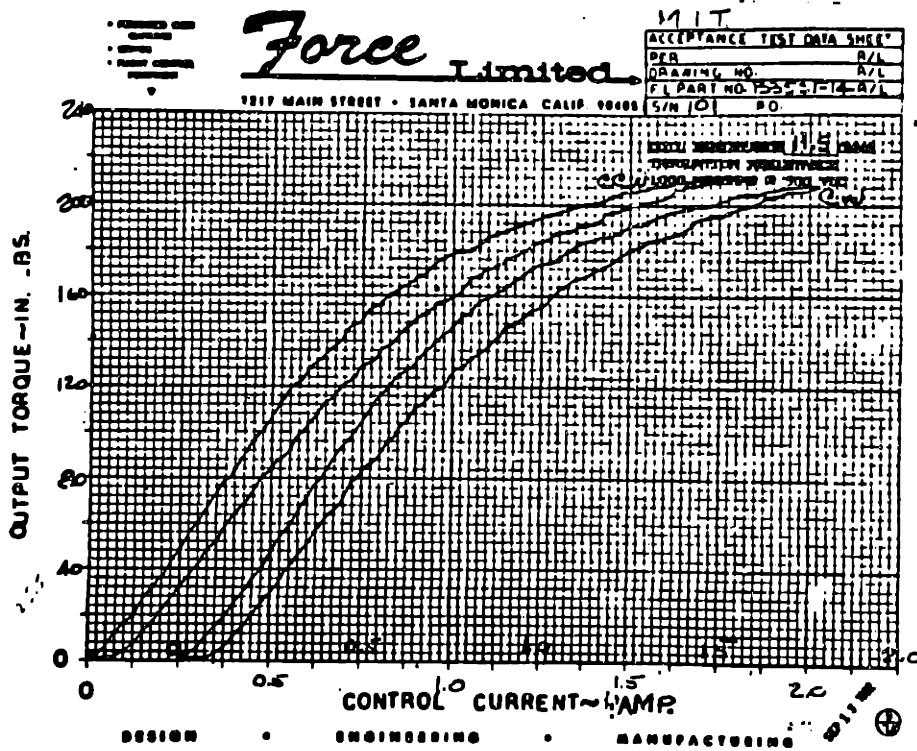
custom made unit by Force Limited. Their brakes had the highest torque-to-inertia ratios and lowest friction of the devices surveyed.

It should be mentioned that a linear version of this device was considered. The positive aspects of a linear device include direct linear action and a significantly higher torque-to-inertia ratio than a rotary vane motor. Unfortunately linear magnetic particle brakes are unavailable and the pneumatic capacitance of an air cylinder may hamper pressure reversal. Other reasons for choosing a rotary motor are ease of modification, availability and cost.

Originally it was assumed that the energizing coil of the particle brake would behave as a large inductor. An experiment, which disproved this assumption, was performed to determine the current flowing through the brake as a function of the input voltage. The voltage input signal originated from a sine wave generator

31

Figure 15. Brake Current Amplitude Response
for a Sinusoidal Vlotage Input

and was amplified by the actual amplifier used in the actuator system. This amp began to distort it's voltage output signal at $15Khz$ with the brake load on it. The current was measured via a one ohm series resistor. The resulting voltage across the resistor was displayed on an oscilloscope along with the input voltage from the amp. Figures 15,16 show the log magnitude and phase plots of the response. As can be seen from the plots there is a break point at about $1Hz$ from the inductive time constant. The additional phase lead and increase in current magnitude are assumed to result from inter-winding capacitance in the brake coil. Note that the maximum phase lag is about -50 degrees and occurs at about $20Hz$.

**Figure 16. Brake Current Phase Shift for a
Sinusoidal Voltage Input**
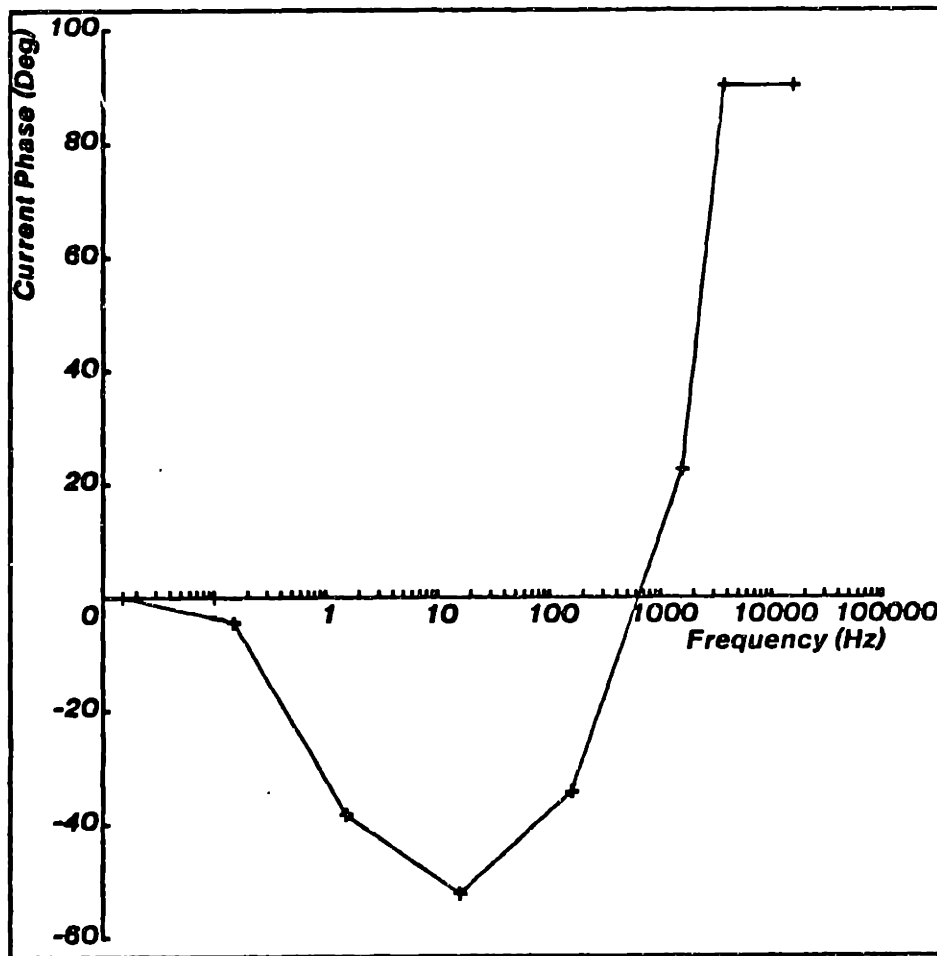
Another experiment was performed to determine the dynamic characteristics of the torque response to a current input. The current input was generated as in the previous experiment. The torque output was not easy measured. Ideally one would measure acceleration and relate that to the applied torque. In lieu of this, measurement was made of the device velocity by monitoring the tachometer output. There were several drawbacks to this. For one, what is being measured is really the integral of the desired measurement. Unfortunately, the integration operation scales the data by a factor proportional to $1/\omega$ where ω is the frequency of the input signal. Another drawback is the problem of mechanical resonances and

electrical noise superimposed on this signal. Additionally, the brake outputs zero torque regardless of current input when there is no external applied torque. This necessitated running the air motor at some torque level. The motor itself has cyclic torque variations due to the action of it's vanes and several mechanical resonances which were excited by the slapping action of the vanes as they were loaded and unloaded by air pressure.

As a consequence of the difficulty of measurement only phase information was obtained for the velocity response to a current input. This is shown in Figure 17 that there is significant phase lag which has a maximum of about -150 degrees at about $25Hz$. This is postulated to be due to response of the magnetic particles in the brake. Adding this phase lag to that for the current response results in a total of about -200 degrees at around $25Hz$. Clearly this situation will require some form of compensation if it is to be included in a closed loop control scheme. Because the MIT assembly robot controller will only run a control loop at $500Hz$ an analog inner loop was closed in order to compensate for the phase lag and to roll off the response at high frequency.

Figure 17. Actuator Velocity Output Phase
Shift for a Sinusoidal Current Input
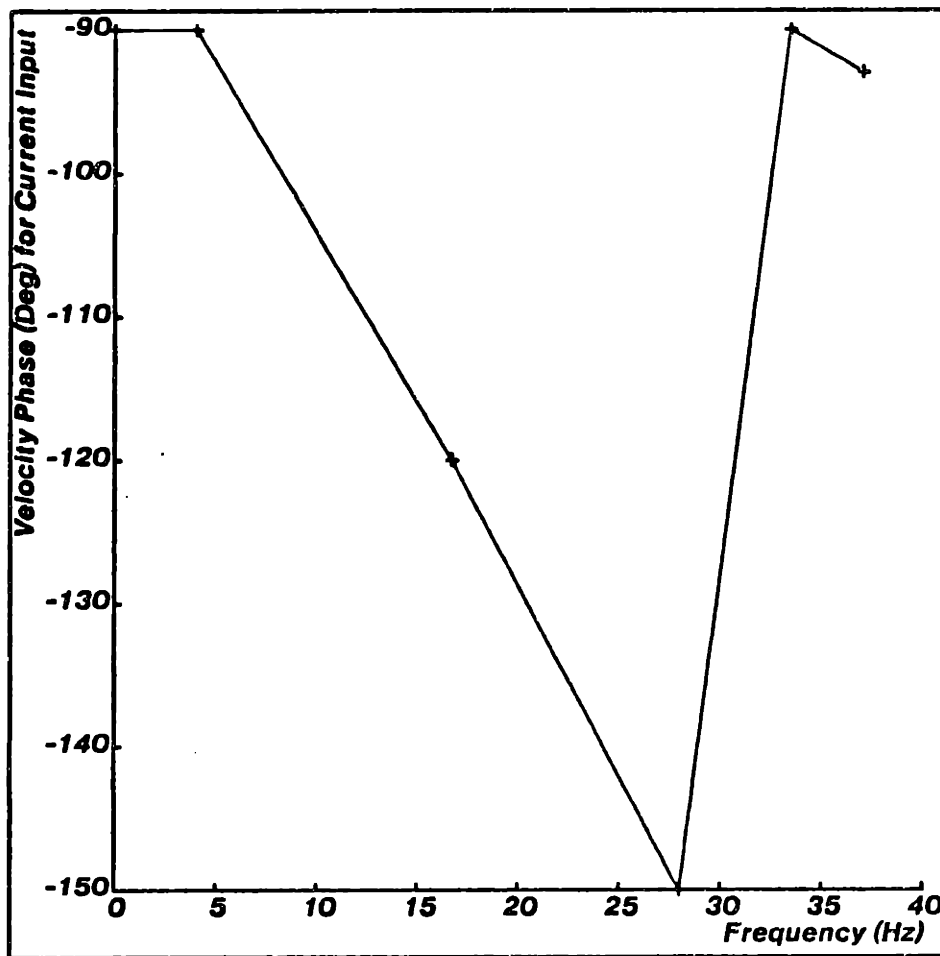
4. Brake Compensation Controller Design

The schematic for this controller is shown in Figure 18. The command signal and the velocity feedback signal from the tach are first passed through a lowpass filter with a cutoff frequency of $300Hz$ before being output to the power amplifier. The tach signal is also fed into a stable analog differentiator circuit. This differentiator supplies the necessary phase lead to compensate for the previously mentioned -200 degree phase shift. The circuit acts like a differentiator at low frequencies but also rolls off at 20db per decade at high frequencies. The peak of the rather triangular

Figure 18. Analog Loop Velocity Controller
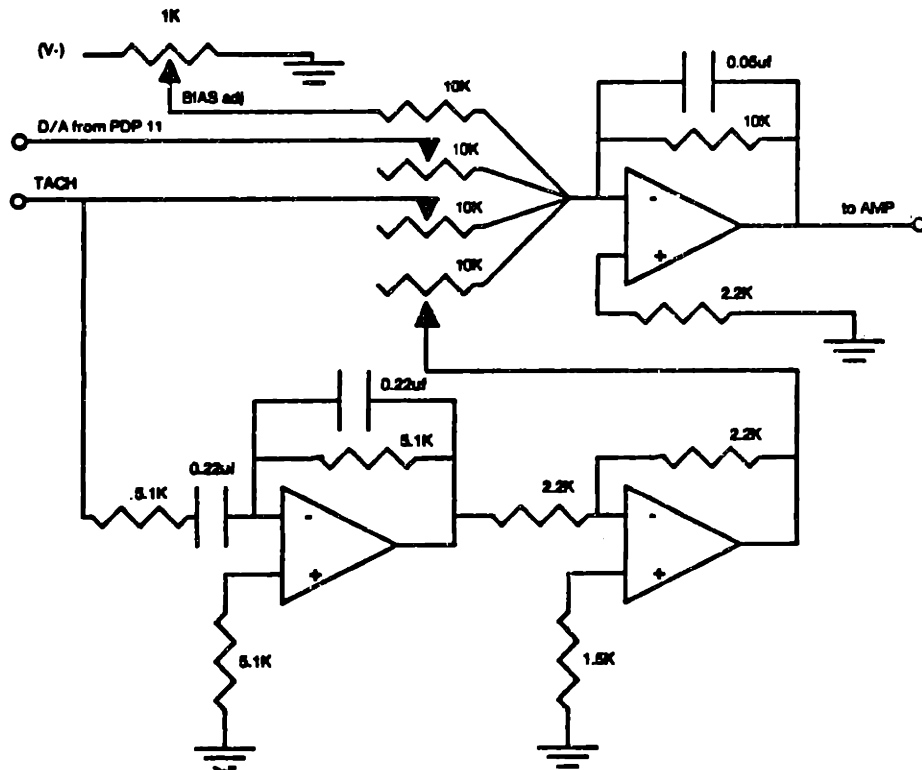
looking frequency response of this filter was set at $150Hz$. The circuit includes four adjusting pots; one to set the gain on the velocity input signal, another one to set, the velocity feedback "stiffness", a third to adjust the amount of velocity damping (or acceleration feedback), and a forth one to set a bias torque to counteract the stall torque of the air motor.

This circuit was adjusted by increasing the velocity stiffness until it could no longer be stabilized by increasing the damping. Then the bias was set to balance the motor stall torque. The D/A gain was then set such that at full scale the motor ran at approximately $2000Rpm$.

A frequency response test was then performed on the velocity servo which yielded the data shown in Figures 19 and 20. Notice that it behaves much like a second order plant with a natural frequency of $3Hz$ and a 0.2 damping ratio. This

36

Figure 19. Velocity Amplitude Response of Analog Velocity Servo
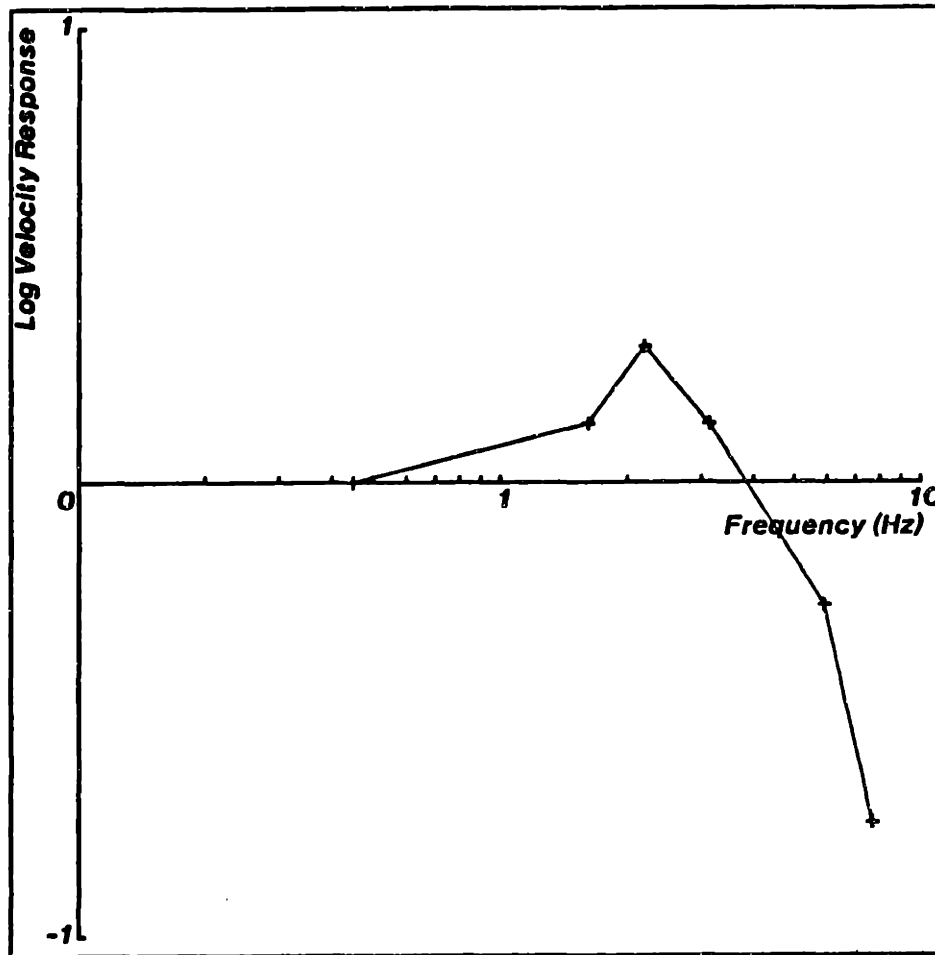
was then included in a closed loop position controller.

4.1. Hybrid Actuator Characteristics

In a DC servo system utilizing proportional or proportional plus derivative control the servo system stiffness is defined as the ratio of motor torque to error signal. In order to generate a torque there must be an error signal. With PID control there must at least be a transient error signal so that the integrator can increase the control signal to the point of nulling the error signal. In some systems this servo stiffness is the most compliant component.

The proposed actuator system will be capable of generating full torque with

Figure 20. Velocity Phase Response of Anolog Velocity Servo

virtually no error signal simply by commanding maximum brake torque. This would be very useful for maintaining a desired position.

I will now derive a set of idealized theoretical operating curves for the actuator and use them to support the hypothesis that over a useful limited range of operation it behaves much the same as a DC permanent magnet motor.

Figure 21 shows an idealized torque/speed curve for an air motor operating at pressure $P1$. Torque T_{stall} is the idealized motor's stall torque and the ω axis intercept is the no load speed. Curves for pressures less than $P1$ are parallel to and lie below the one shown.

## Figure 21. Ideal Air Motor Torque/Speed Curve
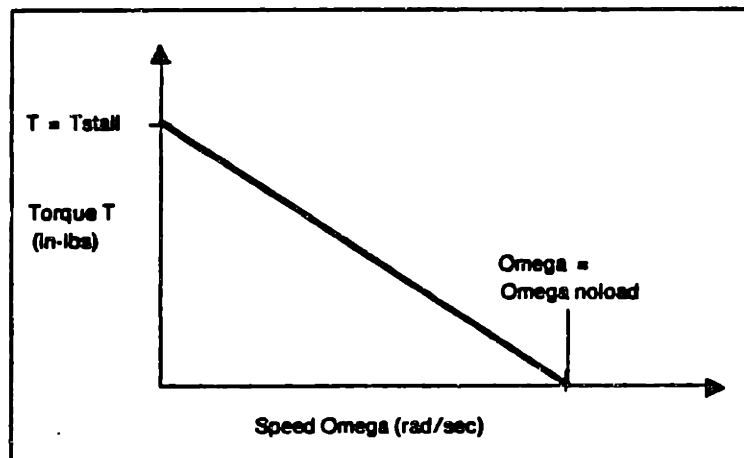
Figure 22 shows the torque/current curve for an idealized magnetic particle brake. This device is much like a disc brake, but with the caliper assembly replaced by an electromagnet and with the clearance space between the magnet and disc filled with a ferrous powder. When the magnet is energized some level of coloumbic friction is developed within the powder between the disc and magnet poles. Note that when $\omega = 0$ the output torque may not lie on one of the curves. In this case the torque lies between the operating points on the two curves for the given current and is opposite in sign to the applied torque.

If we now change the brake current signal to be

$$\left(i_{brake} = i_{off} - i_{cmd} \right)$$

we get a new operating curve shown in Figure 23 with i_{cmd} as input. We will also require that $i_{cmd} \leq i_{off}$. This will insure that the torque is monotonic with command current. When the equality is satisfied the device is in a state of positive saturation (or minimum braking). This positive saturation constraint was

# Figure 22. Ideal Magnetic Particle Brake Torque/Current Curve
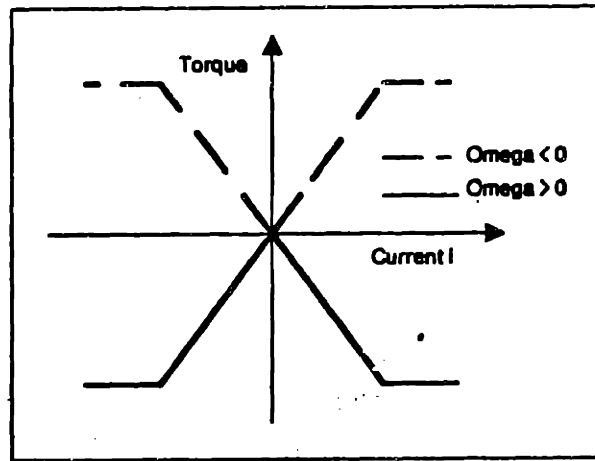
implemented in hardware via a power diode in series with the brake coil. Negative saturation (or full braking) occurs at $i_{cmd} = i_{off} - i_{brakemax}$. In the transformed curve, i_{off} was chosen such that $T1$ equals the stall torque of the air motor.

Combining the air motor curve with the transformed and limited brake curve results in the operating curve for the proposed device shown in Figure 24. Figure 25 shows the operation range of a DC permanent-magnet voltage-controlled motor. Its range is bounded by torque-speed curves for the motor with input voltages of $V1$ and $-V1$. Note that if $\omega > 0$, $T_{stall,hybridsystem} = T_{stall,DCmotor}$ and $-i_{off} \leq i_{cmd} \leq i_{off}$, the operating curves for the hybrid actuator are functionally identical to those of the DC motor.

If $T_{stall,DCmotor}$ is chosen to correspond to the maximum allowable motor current(because of demagnetization, brush current capacity, etc.) then the upper and lower corners of Figure 25 are cutoff for values of $T > T_{stall}, T < -T_{stall}$. In this case the hybrid actuator has a larger operating region. If, in addition we let $i_{cmd} = i_{off} - i_{brake-max}$ (negative saturation) then the operating region is greatly

40

Figure 23. Transformed Torque/Current Curve for Particle Brake
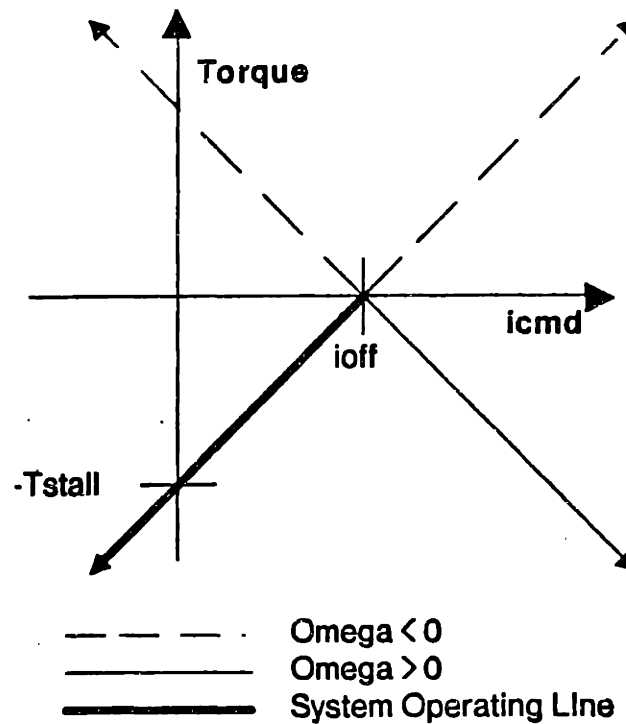
increased. In this case the attainable deceleration can be many times greater than the acceleration.

Note that moving around to different curves in this operation region requires only modulation of the brake current; motor air pressure remains equal to $P1$. Therefore, we should be able to place this device into a closed loop servo system replacing the DC drive, provided that the control system does not require the device to back up. In other words, the velocity must not change sign during a move.

The region of Figure 24 in which $\omega < 0$ corresponds to the situation in which the device is backdriven. Here the brake torque adds to the motor torque producing a sharp discontinuity at $\omega = 0$. The controller must be programmed to avoid

Figure 24. Torque Speed Curves for the Hybrid System
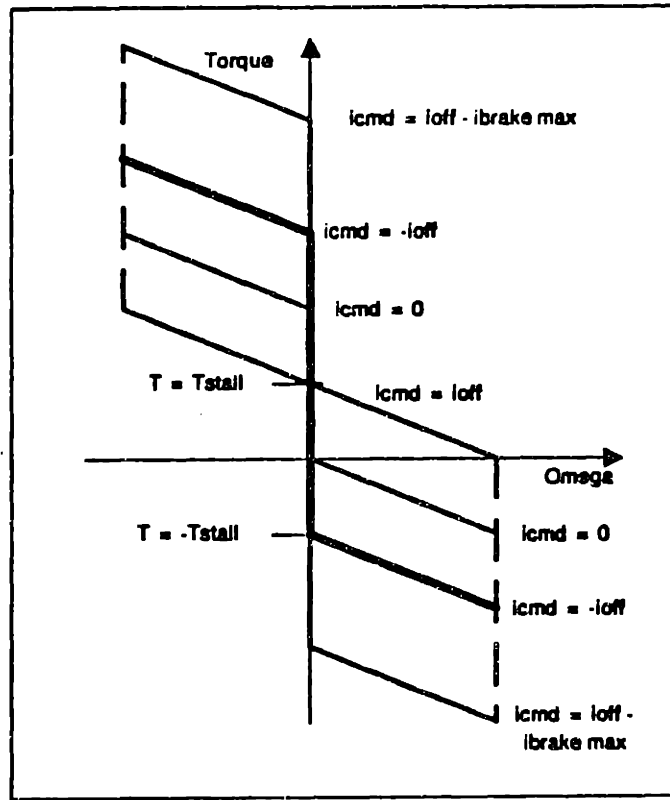
operation through this discontinuity.

The basic mode of operation of this device will be to turn the air motor full on to produce maximum torque in one direction with the opposing torque level in the brake producing a net output torque of zero. A position feedback loop will be closed around the brake such that an increasing error signal will result in decreasing brake torque thus allowing the device to accelerate. In this manner, the brake will be made to appear to the servo system as a torque source instead of a sink.

Figure 25. Range of Operation of a Voltage Controlled DC Motor
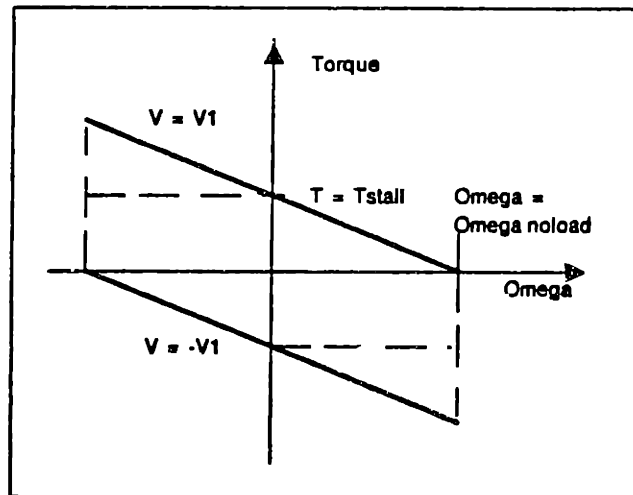
5. Controller Design

Block Diagram

A linearized block diagram of the hybrid servo system is shown in Figure 26. Notice that we have assumed full state feedback, which is represented by the derivatives in the feedback path. The system shown here is of third order and will require some analysis.

5.1. 3rd Order System Analysis

Overview

In the following section various criterion which relate to the roots of eq(28) as functions of the coefficients A and B will be presented. Among these criterion are Rouths Stability, All Real Roots, No Velocity Reversal, and choices of coefficients A,B corresponding to ITAE, Butterworth, All Real And Equal and Phelan root choices. These will be followed by a development of a constrained (no velocity reversal) ITAE minimization. A series of step response time simulations along the border of the no velocity reversal region have been run. These time simulations

Figure 26. Linearized Block Diagram of System

Figure 26. Linearized Block Diagram of System
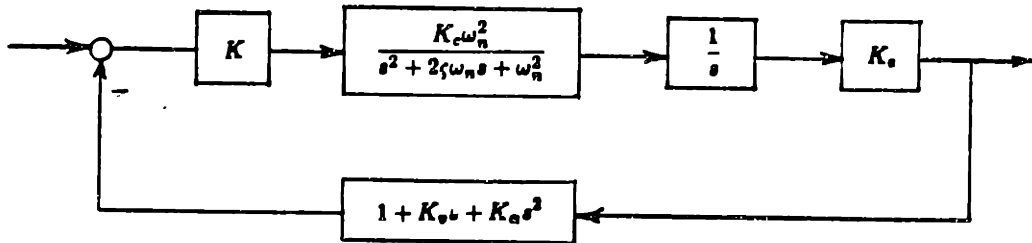
serve as the basis for choosing A and B.

Criteria for Root Choice

The characteristic equation for a linear third order system can be written in the following form.

$$s^3 + A\omega s^2 + B\omega^2 s + \omega^3 = 0 \tag{28}$$

The following chart summarizes several criteria relating to choice of coefficients for eq(28). The first five can be found in the literature while and the remaining

44

three are developed in the following pages. .

Case	A	B
Routh's Criterion	> 0	$> 0, \quad > 1/A$
Butterworth	2	2
Phelan	2.15	2.32
Equal Real Roots	3	3
ITAE	1.75	2.15
Constrained ITAE	2.07	2.40
Three Real Roots	$\frac{\omega_1 + 2\omega_2 B}{(\omega_1\omega_2^2)^{1/3}}$	$\frac{2\omega_1\omega_2 + \omega_2^2}{(\omega_1\omega_2^2)^{2/3}}$
No Velocity Reversal	$\frac{2\zeta + \dot{\omega_1}}{\dot{\omega_1}^{1/3}}$	$\frac{1 + 2\zeta\dot{\omega_1}}{\dot{\omega_1}^{2/3}}$

The Rouths, Real-Root and No-Velocity-Reversal loci are plotted in Figure 27 along with the ITAE, Butterworth and Phelan points. Another version of this graph by Meyfarth[17], Figure 28, shows the mapping of first and second order system coordinates into the A,B plane.

Routh's stability criterion, in this case, determines over what range of coefficient combinations the solution of eq(28) is stable. Notice that stable solutions exist only in the first quadrant of the A,B plane in a region to the right of the hyperbola $AB = 1$.

A third order system may be thought of as a cascade of a first and a second order system. If one takes this point of view, the case of borderline three real roots may be found by setting the damping ratio of the second order system to unity, expanding the characteristic equation and equating coefficients to those of eq(28). The step response of a third order system with all real roots exhibits no overshoot, however the response may not be "optimal".

Figure 27. System Root Characteristics as a Function of A,B
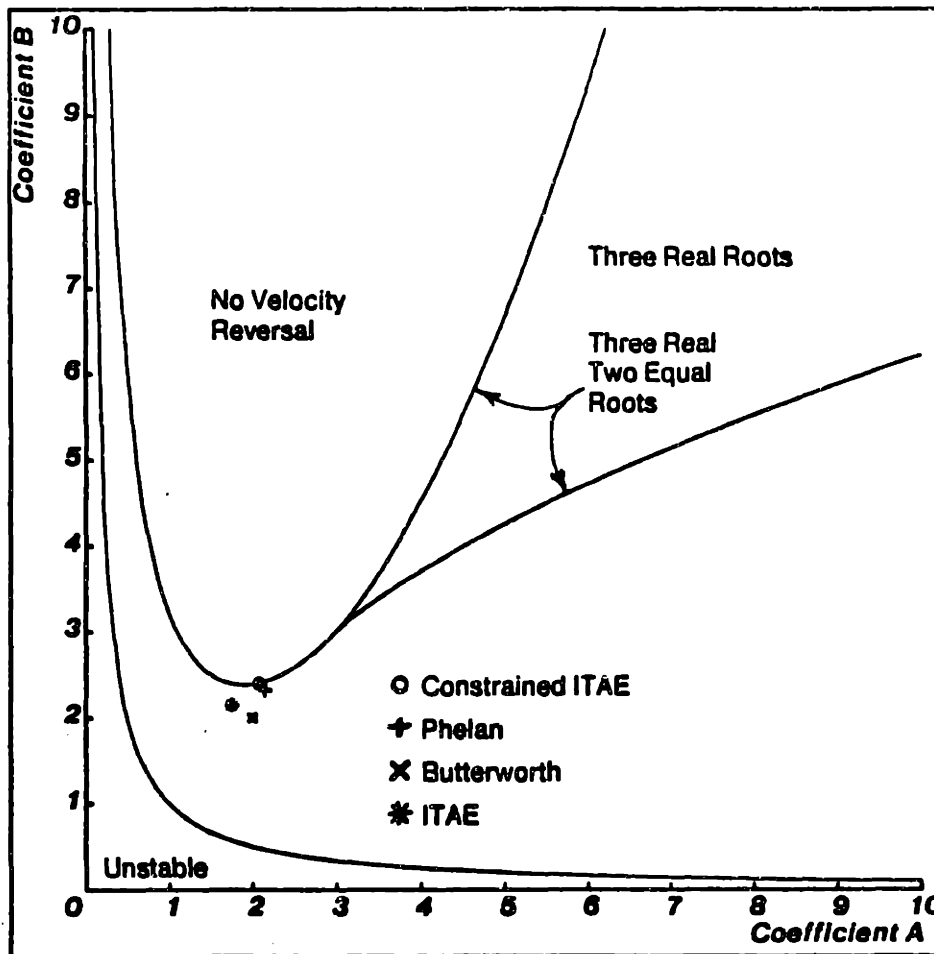
The ITAE root choice (Integral Time Absolute Error) results in time optimal response for a given value of $\omega^3 = \omega_1\omega_2^2$. There is overshoot in this time response making the system dynamics incompatible with the hybrid actuator. This point is presented mainly for comparison.

The Butterworth 3rd order filter root choice yields a transfer function with maximally flat frequency response; but, unfortunately overshoots in the time response. Notice that the coefficients A and B lie on a line with endpoints at the origin and the cusp of the Real Root region of Figure 27. Coefficients lying on this line correspond to the locus of poles on a circle of radius ω in the S plane. The

Figure 28. Mapping of First and Second Order
System Coordinates into the A,B Plane [17]
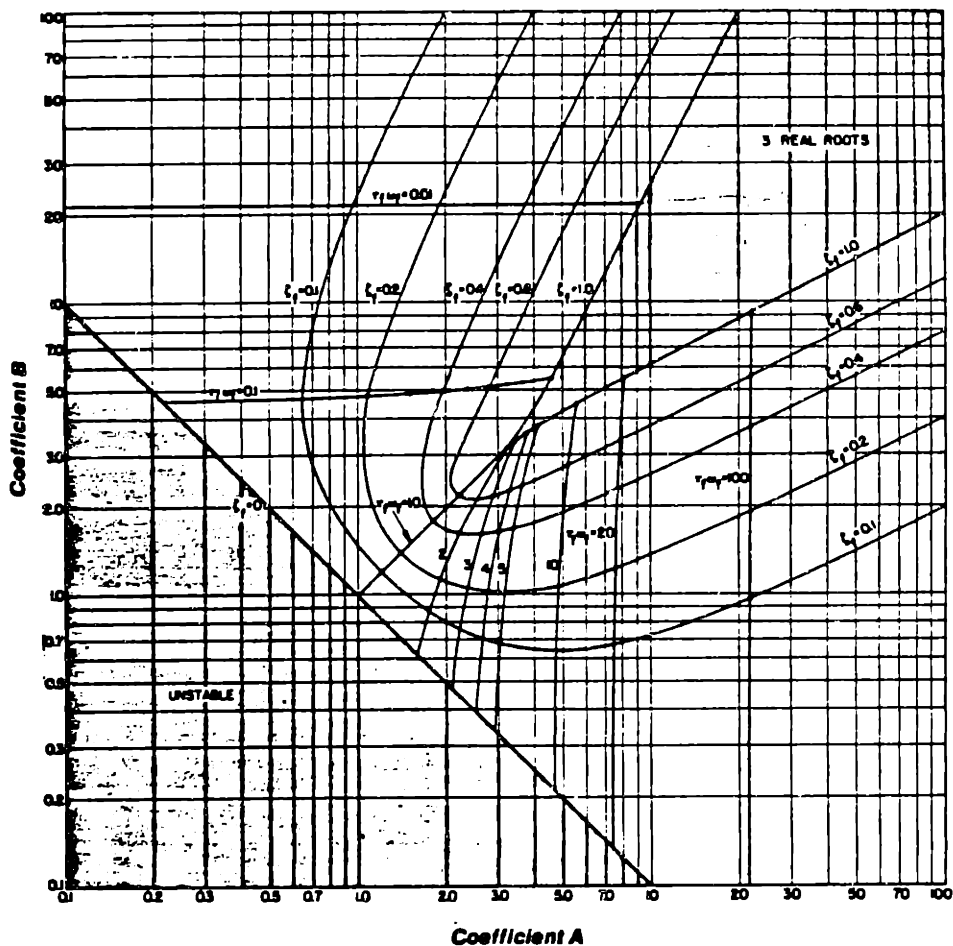
cusp of the Real Root region corresponds to three coincident poles at $-\omega$. At the crossing of Rouths Criterion there is one root at $-\omega$ and two pure imaginary ones at $\pm i\omega$.

Moving to the right from the Butterworth point makes the first order pole faster and the second order ones slower in keeping with $\omega^3 = \omega_1\omega_2^2$. Note, from root locus analysis slower poles tend to have larger residues and hence greater dominance in the response.

Moving up from the Butterworth point makes the 2nd order poles faster and

the first order one slower.

Phelan Criterion

The Phelan controller is obtained through application of the following two specifications for performance.

(a) The fastest possible response to a step change in reference input without overshoot and without oscillation.

(b) The least change in the value of the controlled variable (output) and the quickest recovery when the controlled system is subjected to a step load.

Note, condition (a) relates to pole placement and (b) to pole placement and topology.

The topology of a Phelan controller for a second order system is that of a second order system with full state feedback surrounded by an additional position feedback loop with pure integral control. This pure integral controller results in the system's order being increased to three. In mapping the Phelan controller of a second order system to that of the third order system being considered, condition (a) is preserved but condition (b) is not.

Overdriven Phelan Controller

We need a few variables for this discussion; r_0 =reference step input, $r_{0,ml}$ = max value of r_0 for which the response will be linear, m =level of one component of power being delivered to the final control elements (typically voltage or current), $(-m_{max} \leq m \leq m_{max})$.

The coefficients of this controller are determined by m_{max} and choice of $r_{0,ml}$. When overdriven (nonlinear operation) the system begins to overshoot when r_0 exceeds about $2.85r_{0,ml}$ provided a smart integrator is used. The smart integrator is defined by the following two conditions.

(c) Output of controller never exceeds m_{max}

(d) When the system recovers to, or reaches, the point at which it can operate linearly the integrator has the correct value, i.e., the correct initial condition to transform from being overdriven to operating linearly.

The proposed device has a larger linear range of operation when stopping than starting and should therefore be tolerant of overdriven operation.

It is not necessary for all the roots to be real to avoid overshoot to a step input. All that is necessary is that the velocity (or impulse response) remain of the same sign throughout the move. The transfer function of a third order system can be thought of as that of cascaded first and second order systems shown below.

$$\frac{w_1 w_2^2}{(s + w_1)(s^2 + 2\varsigma w_2 s + w_2^2)} \tag{29}$$

let

$$w_2^* = \frac{w_2}{w_2} \tag{30}$$

$$w_1^* = \frac{w_1}{w_2} \tag{31}$$

and since we are only concerned with relative frequencies (character of response, not speed of response) let

$$w_2 = 1 \tag{32}$$

then the transfer function becomes

$$\frac{w_1^*}{(s + w_1^*)(s^2 + 2\varsigma s + 1)} \tag{33}$$

Taking the inverse laplace transform of this equation yields the impulse response or velocity response to a step input. Setting this equal to zero and solving for t yields the following two equations. (Note: valid for $0 < \varsigma < 1$ only)

$$e^{-(\varsigma + \overset{\bullet}{w_1})t} = 0 \tag{34}$$

whose solution is $t = \infty$, and

$$(\varsigma - \overset{\bullet}{w_1})\sin\sqrt{1 - \varsigma^2}t = \sqrt{1 - \varsigma^2}(e^{(\varsigma - \overset{\bullet}{w_1})t} - \cos\sqrt{1 - \varsigma^2}t) \tag{35}$$

Now we want one solution at $t = 0$, one at $t = \infty$ and no solution $0 < t < \infty$ for the velocity not to change sign during a move. Having found the one at $t = \infty$ we must next find the one at $t = 0$ and the limiting case of solutions inbetween.

The two sides of eq(35) are each plotted in Figure 29 for a set of values of ς and $\overset{\bullet}{w_1}$ such that $(\varsigma - \overset{\bullet}{w_1}) > 0$. Notice that the curves are tangent at $t = 0$ and diverge thereafter. This conclusion can be verified by examining the derivatives of each side of eq(35) shown below.

$$\sqrt{1 - \varsigma^2}(\varsigma - \overset{\bullet}{w_1})\cos\sqrt{1 - \varsigma^2}t$$

$$\sqrt{1 - \varsigma^2}((\varsigma - \overset{\bullet}{w_1})e^{(\varsigma - \overset{\bullet}{w_1})t} + \sqrt{1 - \varsigma^2}\sin\sqrt{1 - \varsigma^2}t)$$

In the limit as t approaches 0 both of these equations become equal to the quantity

$$\sqrt{1 - \varsigma^2}(\varsigma - \overset{\bullet}{w_1})$$

Zeta = 0.5, Omega$\overset{*}{_1}$ = .35
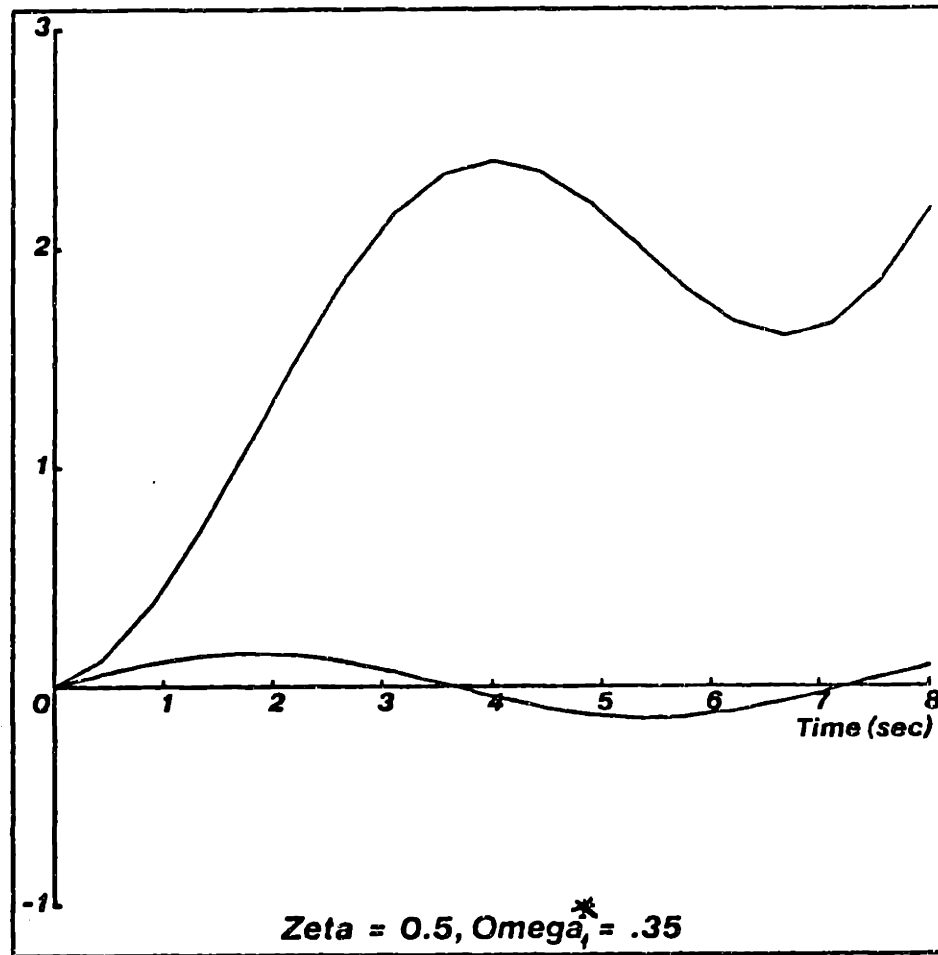
The Figure illustrates that for these conditions there is one solution to eq(35) at $t = 0$.

Figure 30 shows plots of both sides of eq(35) for $(\varsigma - \overset{*}{w_1}) = 0$. In this case the curves are periodically tangent which means the impulse response, or the velocity in the step response, goes to zero in the interval $0 < t < \infty$ but is never negative. This is the limiting case.

Figure 31 illustrates the case of $(\varsigma - \overset{*}{w_1}) < 0$ which has many solutions or times at which the curves cross. This indicates that the impulse response changes sign, implying overshoot in the step response. Note, that this velocity reversal may

Figure 30. Graphical Solution for Zero Velocity $(\varsigma = \omega_1^{\bullet})$

Zeta = Omega$_1^{*}$= 0.5
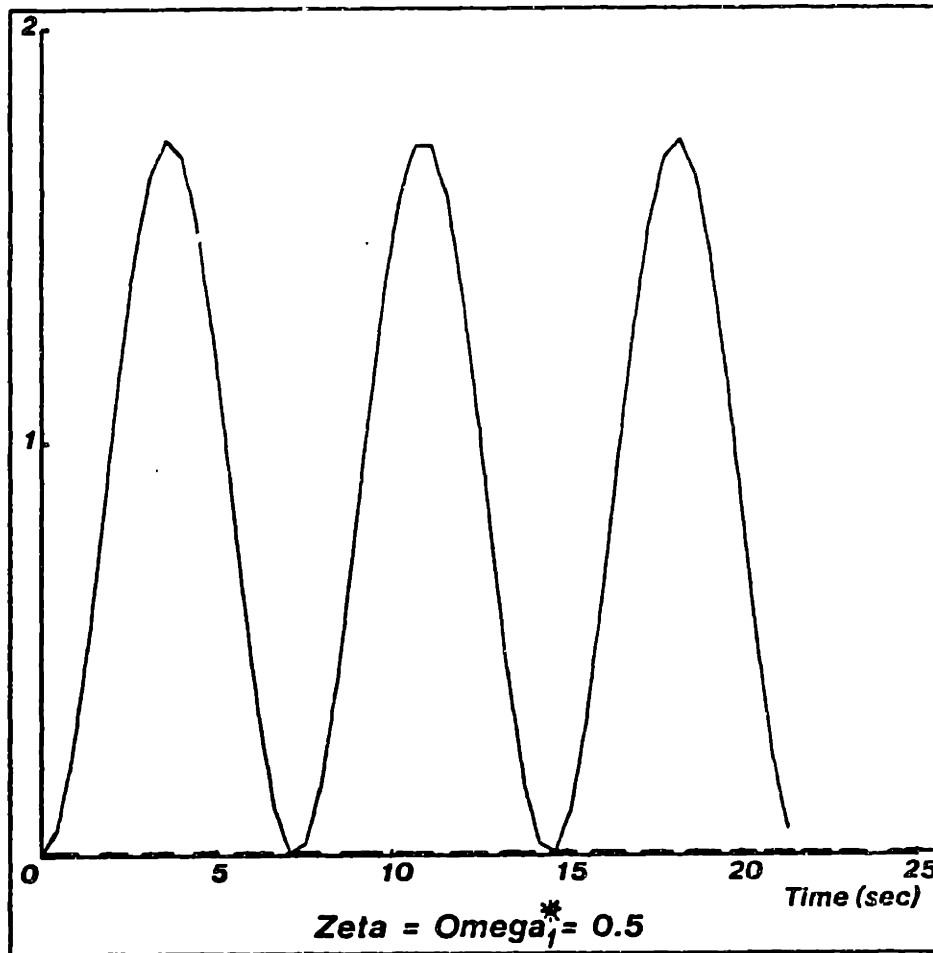
occur inside of a very small exponential envelope.

Stating the limiting no-overshoot case in the first and second order system variables yields.

$$\left(\varsigma - \frac{w_1}{w_2}\right) = 0$$

or

$$\varsigma \omega_2 = \omega_1 \qquad\qquad (36)$$

Figure 31. Graphical Solution for Zero Velocity ($\varsigma < \overset{\bullet}{w_1}$)

Zeta = 0.5, Omega$\overset{*}{_1}$= 1.0
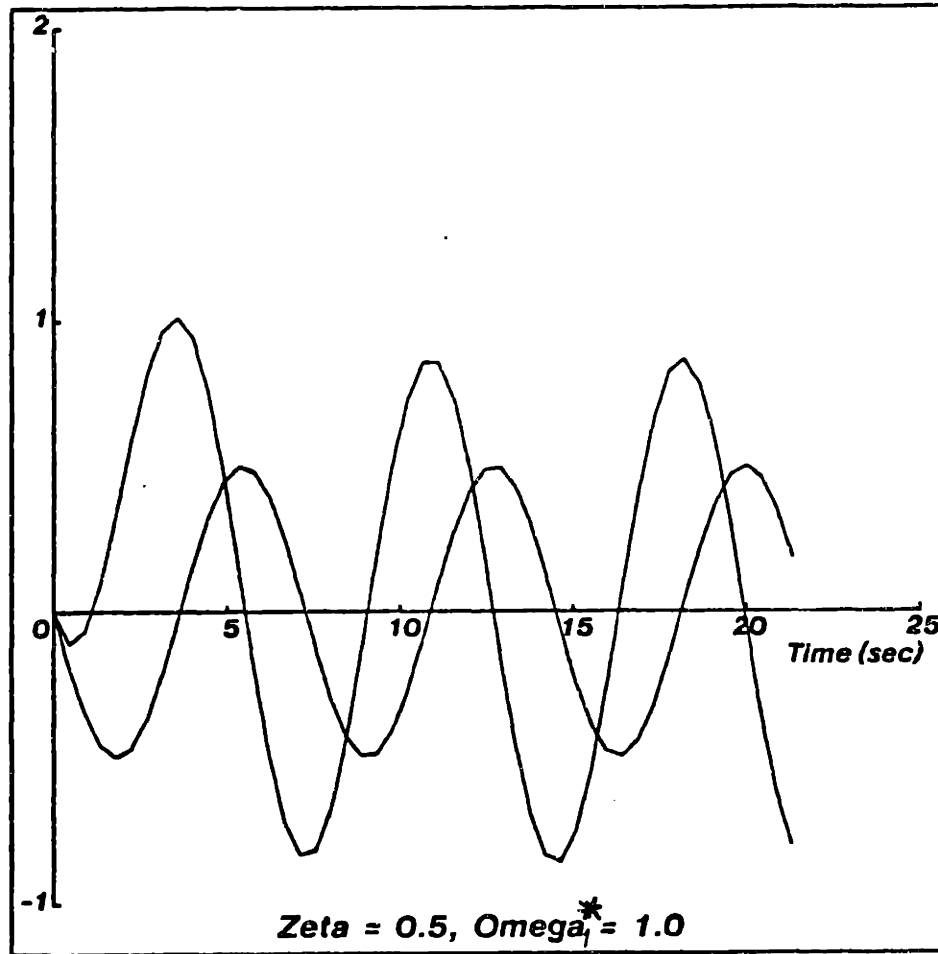
Note that this condition constrains the poles to lie on a vertical line at $-\omega$ in the S-plane.

The following equations obtained from expanding the characteristic equation of eq(33) and equating coefficients to those of eq(28) can be used to transform this limiting case back to coordinates A, B, ω.

$$A = \frac{2\varsigma + \overset{\bullet}{w_1}}{\overset{\bullet}{w_1}{}^{1/3}} \qquad (37)$$

$$B = \frac{1 + 2\varsigma w_1^{\bullet}}{w_1^{\bullet 2/3}} \qquad (38)$$

and letting $\varsigma = w_1^{\bullet}$ with the restriction $0 \leq \varsigma \leq 1$ gives

$$B = \frac{3}{A} + \frac{2}{9}A^2 \qquad (39)$$

with the corresponding restriction $0 \leq A \leq 3$

For a time optimal response with no velocity reversal and hence no overshoot, it is proposed to choose coefficients A, B in the 'two complex one real root with no velocity reversal' region and closest to the ITAE point.

This is accomplished by constraining the following integral

$$ITAE = \int_0^{\infty} t|Error|dt \qquad (43)$$

(where $Error = 1 -$unit step response)

to lie on the edge of the no-velocity-reversal region by, normalizing the frequency, and by subsequently minimizing the integral.

The constraints can be stated mathematically as follows

$$\varsigma = \frac{\omega_1}{\omega_2} \qquad (44)$$

$$\omega^3 = \omega_1 \omega_2^2 = Constant \qquad (45)$$

The constant was arbitrarily chosen to be 1.

Imposing these two constraints on a third order system leaves the transfer function depending on only one parameter. This parameter was chosen to be ς and

Figure 32. Constrained ITAE Optimization
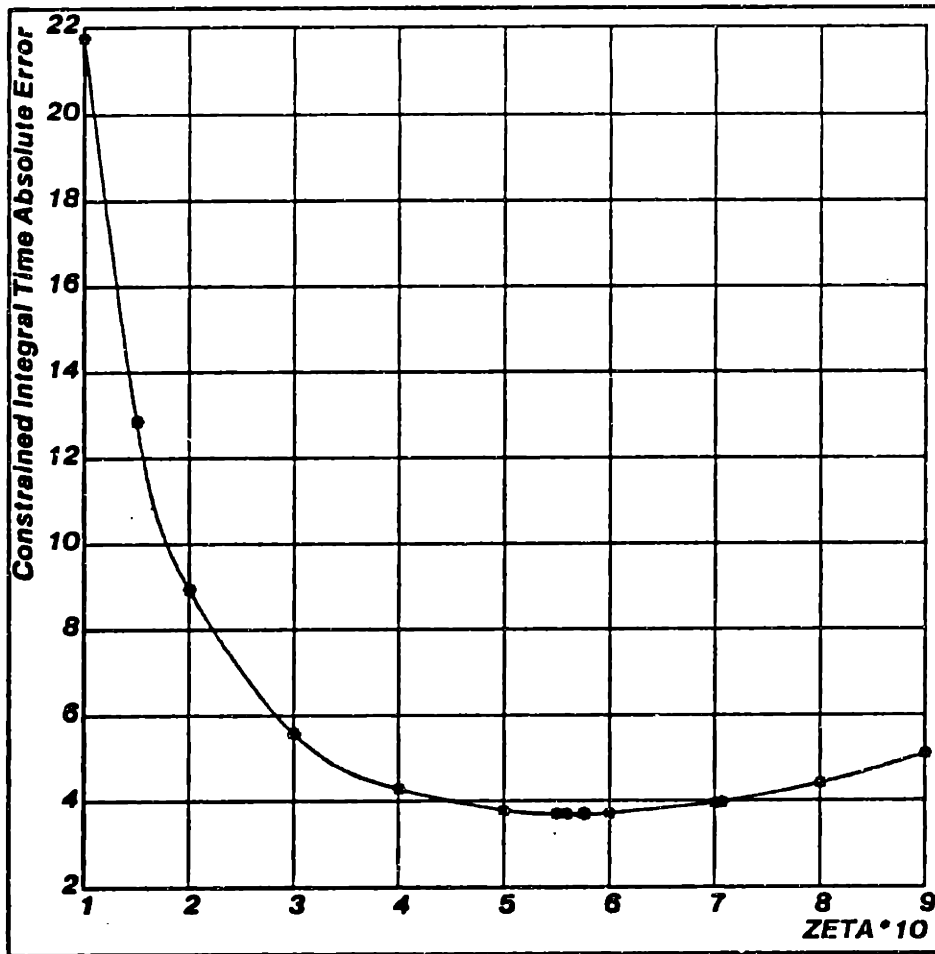
the integral of eq(43) was evaluated for various points in the interval $0.1 < \varsigma < 0.9$. The results are plotted in Figure 32 with the minimum ITAE occurring for ς approximately 0.575.

Combining eqs(37,38) with the constraints (44,45) gives the values of A and B for minimum constrained ITAE.

This analysis suggests that "optimal" equally dominant poles give "better" response than a dominant second order pair for a given ω^3. The natural frequencies of the open loop and closed loop poles is related to the normalized closed-loop loop-gain in Type-One or higher systems by the following formula.

Figure 33. Coordinates Along Border of No Velocity Reversal Region

A=	0.1500000	B= 20.00500	ZETA= 1.1180339E-02
A=	0.3000000	B= 10.02000	ZETA= 3.1622775E-02
A=	0.4500000	B= 6.711667	ZETA= 5.8094747E-02
A=	0.6000000	B= 5.080000	ZETA= 8.9442715E-02
A=	0.7500000	B= 4.125000	ZETA= 0.1250000
A=	0.9000000	B= 3.513334	ZETA= 0.1643168
A=	1.050000	B= 3.102143	ZETA= 0.2070628
A=	1.200000	B= 2.820000	ZETA= 0.2529822
A=	1.350000	B= 2.627222	ZETA= 0.3018692
A=	1.500000	B= 2.500000	ZETA= 0.3535534
A=	1.650000	B= 2.423182	ZETA= 0.4078909
A=	1.800000	B= 2.386667	ZETA= 0.4647579
A=	1.950000	B= 2.383461	ZETA= 0.5240468
A=	2.100000	B= 2.406571	ZETA= 0.5856620
A=	2.250000	B= 2.458333	ZETA= 0.6495190
A=	2.400000	B= 2.530000	ZETA= 0.7155418
A=	2.550000	B= 2.621471	ZETA= 0.7836612
A=	2.700000	B= 2.731111	ZETA= 0.8538150
A=	2.850000	B= 2.857631	ZETA= 0.9259455
A=	3.000000	B= 3.000000	ZETA= 1.000000

$$\Pi_{j=1}^{n}\omega_j = K\Pi_{i=1}^{n-n_f}\omega_i \tag{46}$$

where

n = order of the system

n_f = number of free integrators

K = Normalized closed loop gain

ω_j = 1st order pole, or second order natural frequency in closed loop system

ω_i = 1st order pole, or second order natural frequency in open loop system excluding free integrators

For Type-Zero systems, K becomes $K + 1$. This suggests that reasonable response may result from the choice of three real equal roots.

5.2. Computer simulations

Figure 33 displays a list of coordinates A, B and corresponding damping ratios ς along the border of the No Velocity Reversal region of Figure 27. Figure 34 shows a series of step response simulations of the linear model at these parameter values.

Figure 34. Borderline No Velocity Reversal Simulations
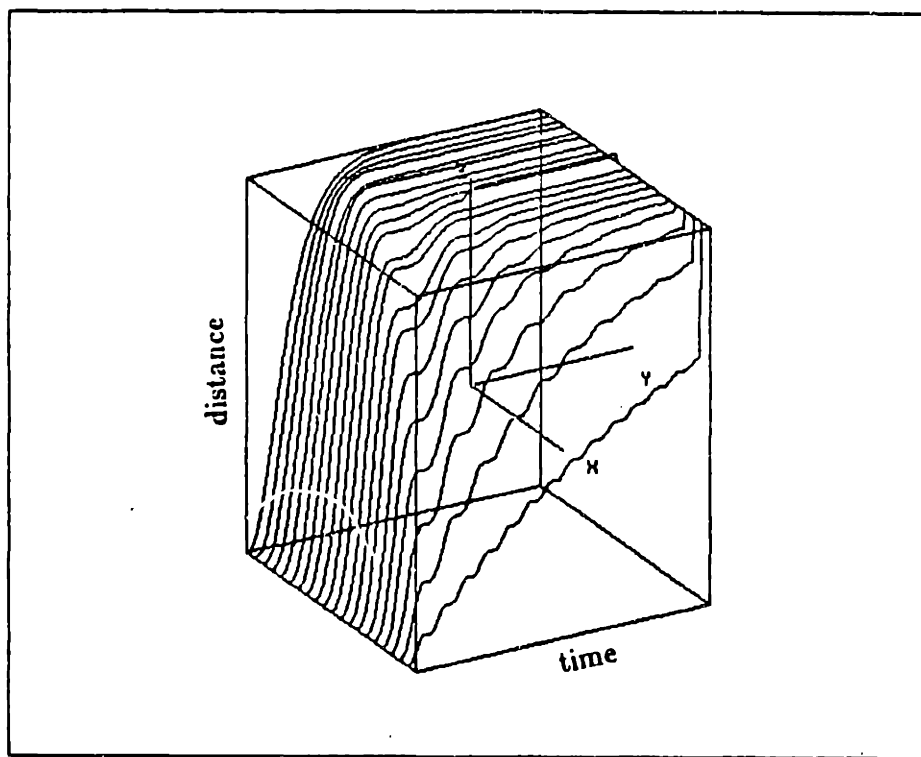
The y dimension corresponds to time, $0 < t < 0.13s$; the z dimension corresponds to output position, $0 < z < 50counts$; and the x value represents simulation number. The simulation at minimum x corresponds to $A, B = 3$. Note that settling time improves for about the first seven simulations moving away from the $A, B = 3$ point before the character of the response gets wiggly.

The simulation corresponding to the constrained ITAE choice of $A = 2.07, B = 2.40$ lies between the seventh and eighth curves counting from the back of the cube. It is interesting to observe that the velocity goes to zero or almost goes to zero before settling to the final value. This makes this choice of controller undesirable because of possible stiction problems.

Figure 35 shows the same set of simulations but with the addition of non-linearities to the model. These include magnetic hysteresis, quantization of amplifier

Figure 35. No Velocity Reversal Simulations with Non Linearities
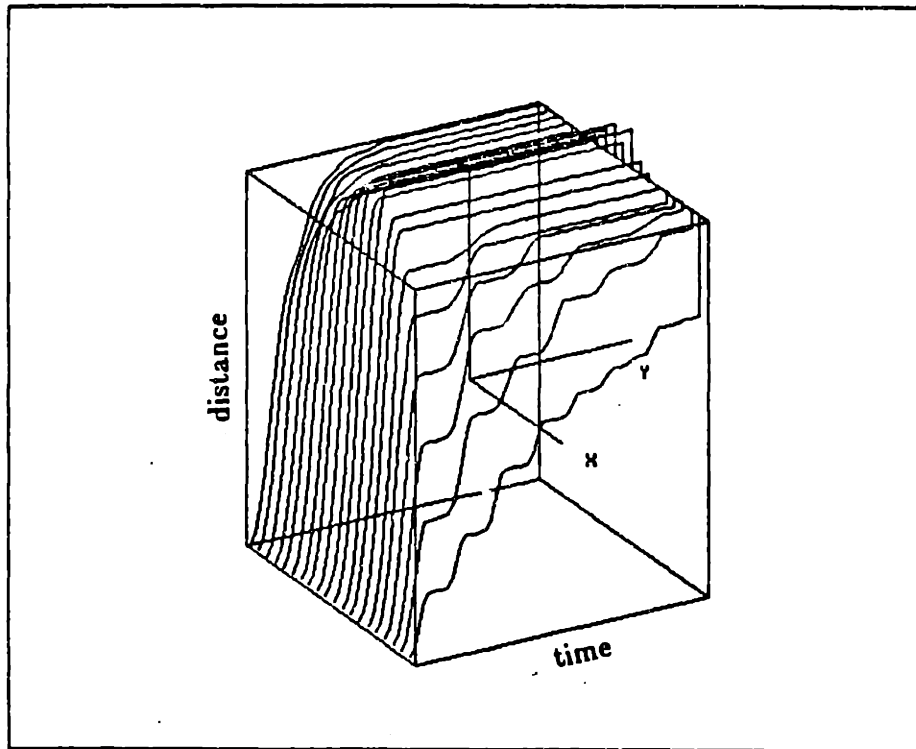
output and encoder input, inclusion of the difference equations and the curvature of the torque/current curve of the brake. It appears that the simulation corresponding to $A, B = 3$ is least sensitive to these non-linearities.

Figure 36 displays a list of coordinates A, B and frequency ratio ω_1/ω_2 along the borderline (3 real root)/(1 real, 2 complex) region of Figure 27. Figure 37 shows a series of step response simulations of the linear model at these parameter values. This figure has the same x, y, z conventions as Figure 34.

Notice that the settling time degrades as one moves away from the $\dot{A}, B = 3$ point. Figure 38 shows a repeat of these simulations with the same non-linearities added the the model as earlier. Again it is seen that the simulation corresponding to A,B=3 is least sensitive to these non-linearities. It is proposed to use $A, B = 3$ to determine the controller gains as robustness is given more importance than settling

Figure 36. Coordinates Along Border of Three Real Root Region

A=	3.000000	B=	3.000000	W1/W2=	1.000000
A=	3.323398	B=	3.263016	W1/W2=	2.526316
A=	3.736341	B=	3.582073	W1/W2=	4.052632
A=	4.273249	B=	3.865066	W1/W2=	5.578948
A=	4.736227	B=	4.115515	W1/W2=	7.105263
A=	5.182838	B=	4.340260	W1/W2=	8.631579
A=	5.613802	B=	4.544634	W1/W2=	10.15790
A=	6.030499	B=	4.732542	W1/W2=	11.68421
A=	6.434343	B=	4.906864	W1/W2=	13.21053
A=	6.826614	B=	5.069775	W1/W2=	14.73684
A=	7.208434	B=	5.222950	W1/W2=	16.26316
A=	7.580769	B=	5.367712	W1/W2=	17.78947
A=	7.944453	B=	5.505116	W1/W2=	19.31579
A=	8.300207	B=	5.636024	W1/W2=	20.84211
A=	8.648663	B=	5.761152	W1/W2=	22.36842
A=	8.990368	B=	5.881092	W1/W2=	23.89474
A=	9.325804	B=	5.996349	W1/W2=	25.42105
A=	9.655401	B=	6.107355	W1/W2=	26.94737
A=	9.979538	B=	6.214478	W1/W2=	28.47368
A=	10.29856	B=	6.318040	W1/W2=	30.00000

Figure 37. Borderline Three Real Root Simulations
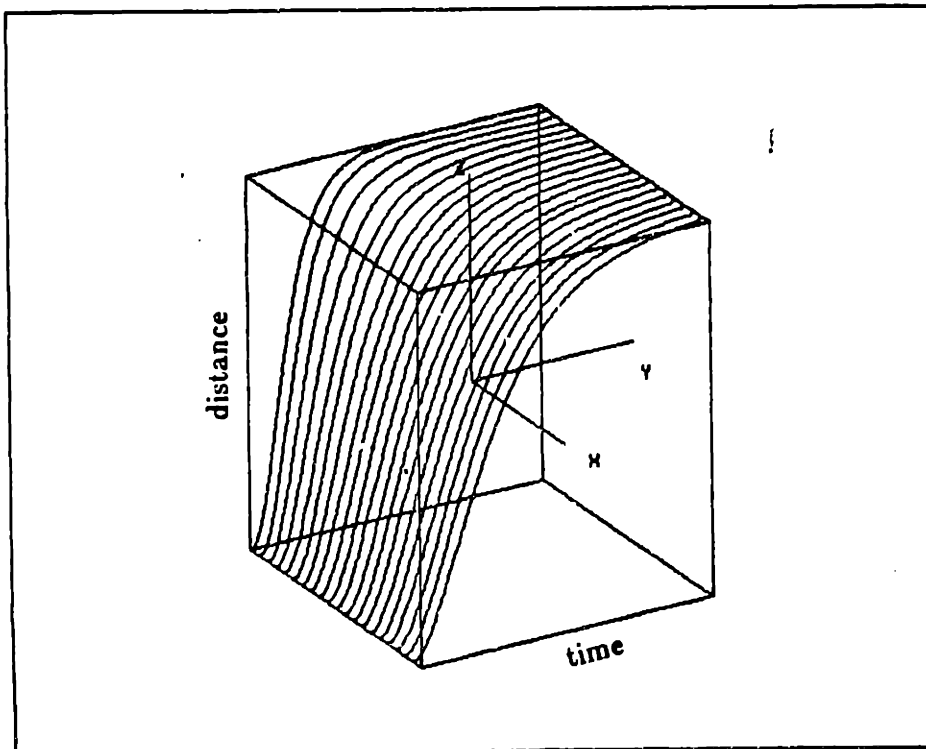
time.

Figure 38. Three Real Root Simulations with Non Linearities
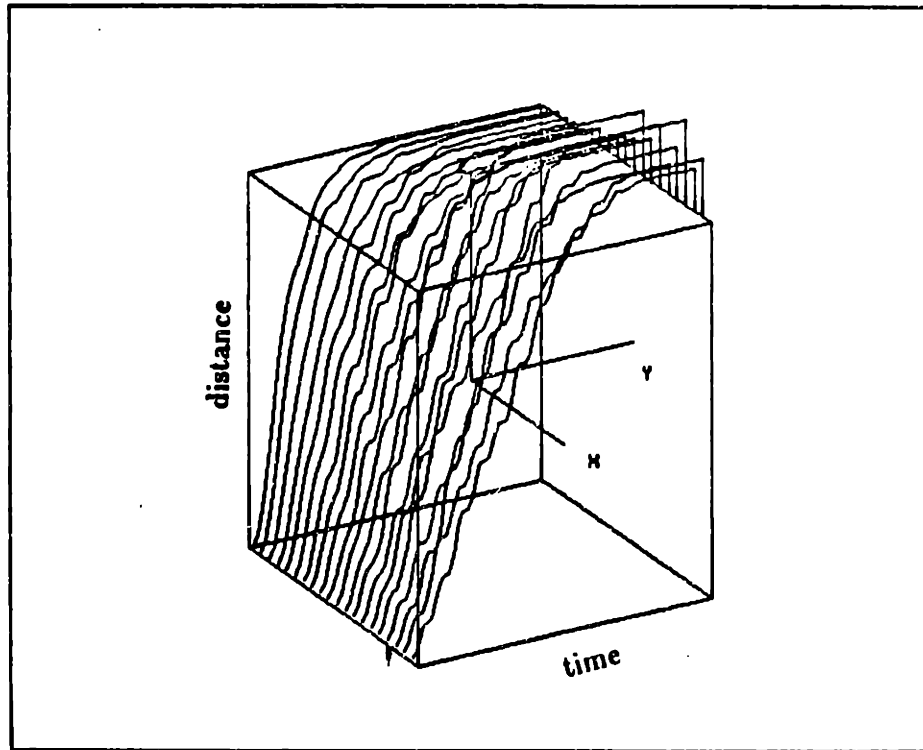
Effect of Large Sample Time

Figure 39 shows a series of simulations of the step response for the linear system with difference equations for a variety of sample periods. The curve at minimum x corresponds to a sample time of $1ms$. The next six curves correspond to sample times of 1.5, 2.0, 2.5, 3.0, 3.5 and $4.0ms$ respectively. A rule of thumb (developed in appendix(i)) suggests that using a sample rate 20 times higher than the highest frequency of interest will result in a reasonable second difference approximation to acceleration. The $2ms$ curve corresponds to the case where the sample rate is 20 times higher than the system cutoff frequency. Performance in this case supports the conclusion of the appendix.

Response to Large Step Inputs

Figure 40 shows the response of the linearized system, with amplifier saturation,

Figure 39. Large Sample Time - 3 Equal Root Step Response
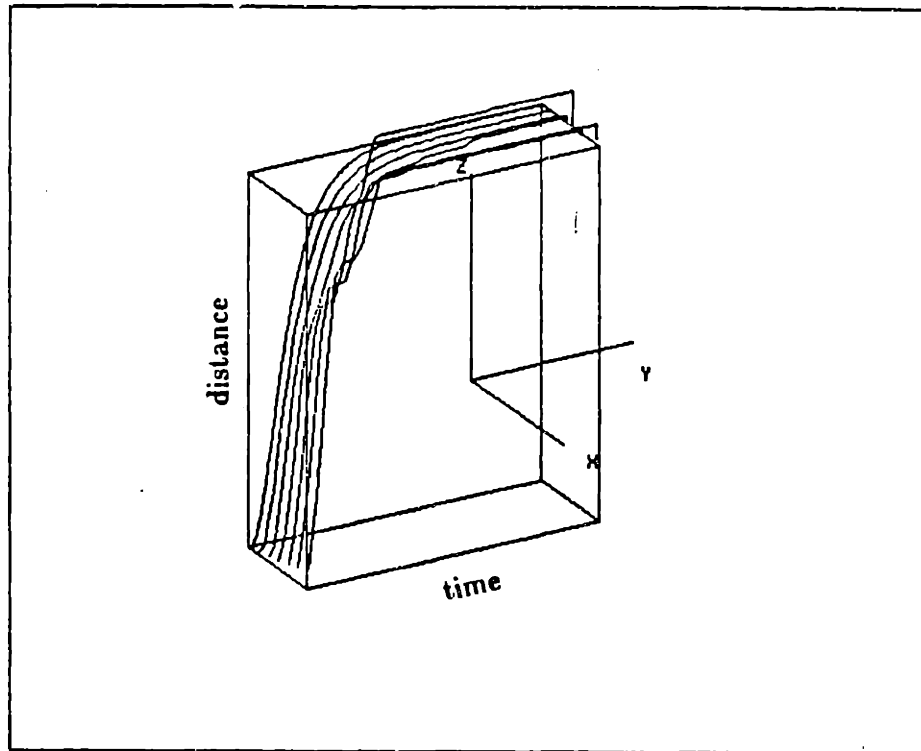
to large step inputs. The curve at minimum x corresponds to a step input of 50 counts. The remaining curves are for steps of 100, 200, 400, 800, 1600, 3200 and 6400counts. The time scale y goes from zero to $0.5sec$. The z scale is normalized from zero to the step size. It is interesting to note that rather large steps can be taken before the system overshoots.

Choice of Controller Gains

Block diagram reduction of Figure 26 yields the following transfer function

$$\frac{K K_c K_e \omega_n^2}{s^3 + (2\varsigma\omega_n + K K_c K_e K_a \omega_n^2)s^2 + (\omega_n^2 + K K_c K_e K_v \omega_n^2)s + K K_c K_e \omega_n^2} \tag{48}$$

and the disturbance transfer function

Figure 40. Effect of Large Step Size
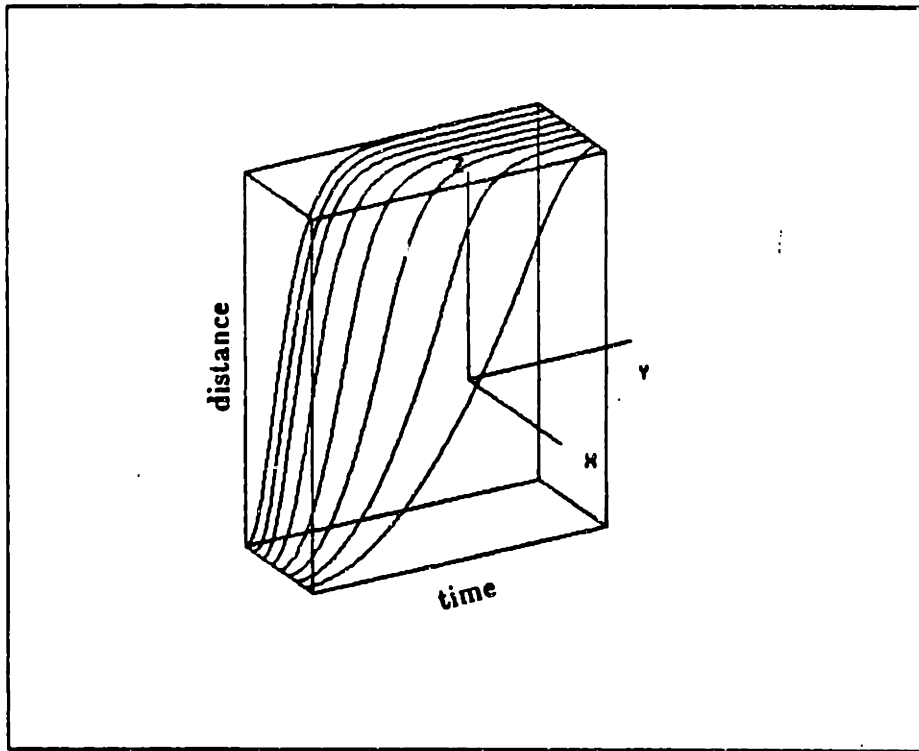
$$\frac{K_e}{s^3 + (2\varsigma\omega_n + KK_cK_eK_a\omega_n^2)s^2 + (\omega_n^2 + KK_cK_eK_v\omega_n^2)s + KK_cK_e\omega_n^2} \qquad (49)$$

Equating coefficients of the characteristic equation to those of eq(28) gives.

$$\omega = (KK_cK_e)^{1/3} \qquad (50)$$

$$B = \frac{KK_cK_eK_v\omega_n^2 + \omega_n^2}{\omega^2} \qquad (51)$$

$$A = \frac{KK_cK_eK_a\omega_n^2 + 2\varsigma\omega_n}{\omega} \qquad (52)$$

The values of system constants are

b =motor viscous damping= $4E - 3FtLbs/rad/s$ when $\omega > 30rad/sec$

b =motor viscous damping= -0.02 when $\omega < 30 rad/sec$

V_{max} =amp power supply voltage= $30 Volts$

K_a=amplifier gain= $\frac{V_{max}}{255} = \frac{30 Volts}{255 counts}$

K_b =brake gain= $\frac{17 FtLbs}{11 Volts}$

$K_e = \frac{636 counts}{Rad}$

$K_c = 1.56 Rad/sec - count$

$\omega_n = 19 Rad/sec$

$\tau = 20ms$

$J = 1.8E - 3 Slugs Ft^2 = 2J_{motor}$

Sample frequency $500 hz$. (fixed by MIT Assy robot architecture)

Calculation of Gains to Meet Specs

Arbitrarily setting the system cutoff frequency to $10Hz$ gives a value for ω in eq(50) of $64 Rad/sec$. Substituting this value and the values of other system constants into eq(50) and then solving for K yields $K = 0.75$. This value of K can now be substituted into eqs(51) and eq(52) along with the selected values of A and B to solve for K_v and K_a.

Figure 41. Experimental Prototype Hybrid Actuator
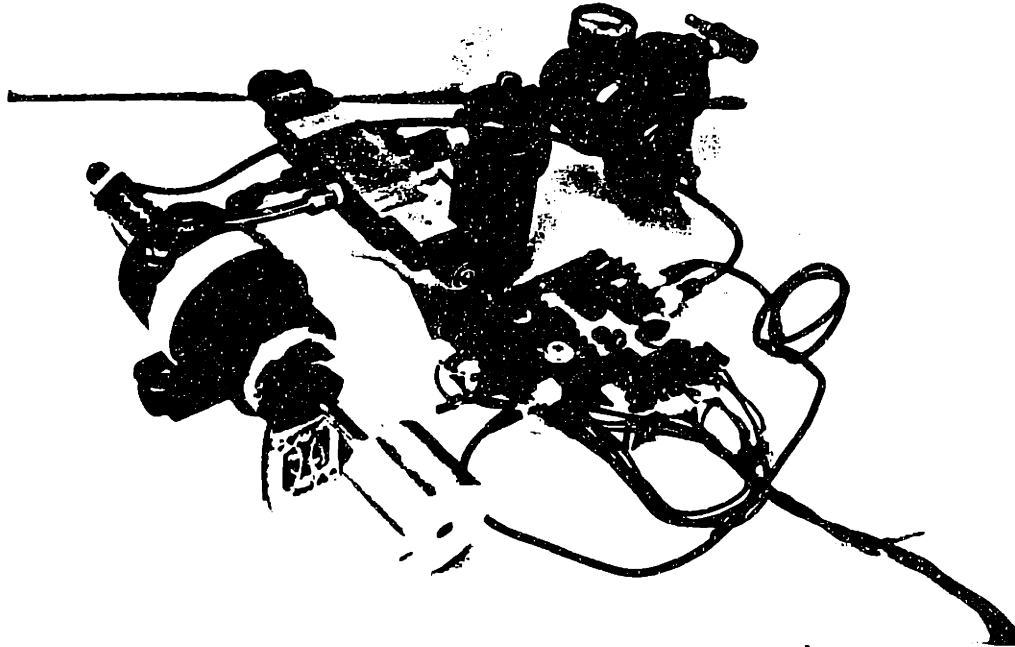
6. Implementation

System Architecture

The overall experimental control system architecture is shown in Figure 42. This is a subset of the MIT assy robot controller hardware. The control program is, in actuality, an interrupt service routine which executes in response to interrupts generated by a real- time clock operating in repeat mode. A reasonable interrupt interval was found to be 2 ms for my particular control routine.

The Intel 8031 micro processor runs an encoder update program at a approximately 2Khz. During each update cycle it reads an 8 bit register of

Figure 42. Overall System Architecture
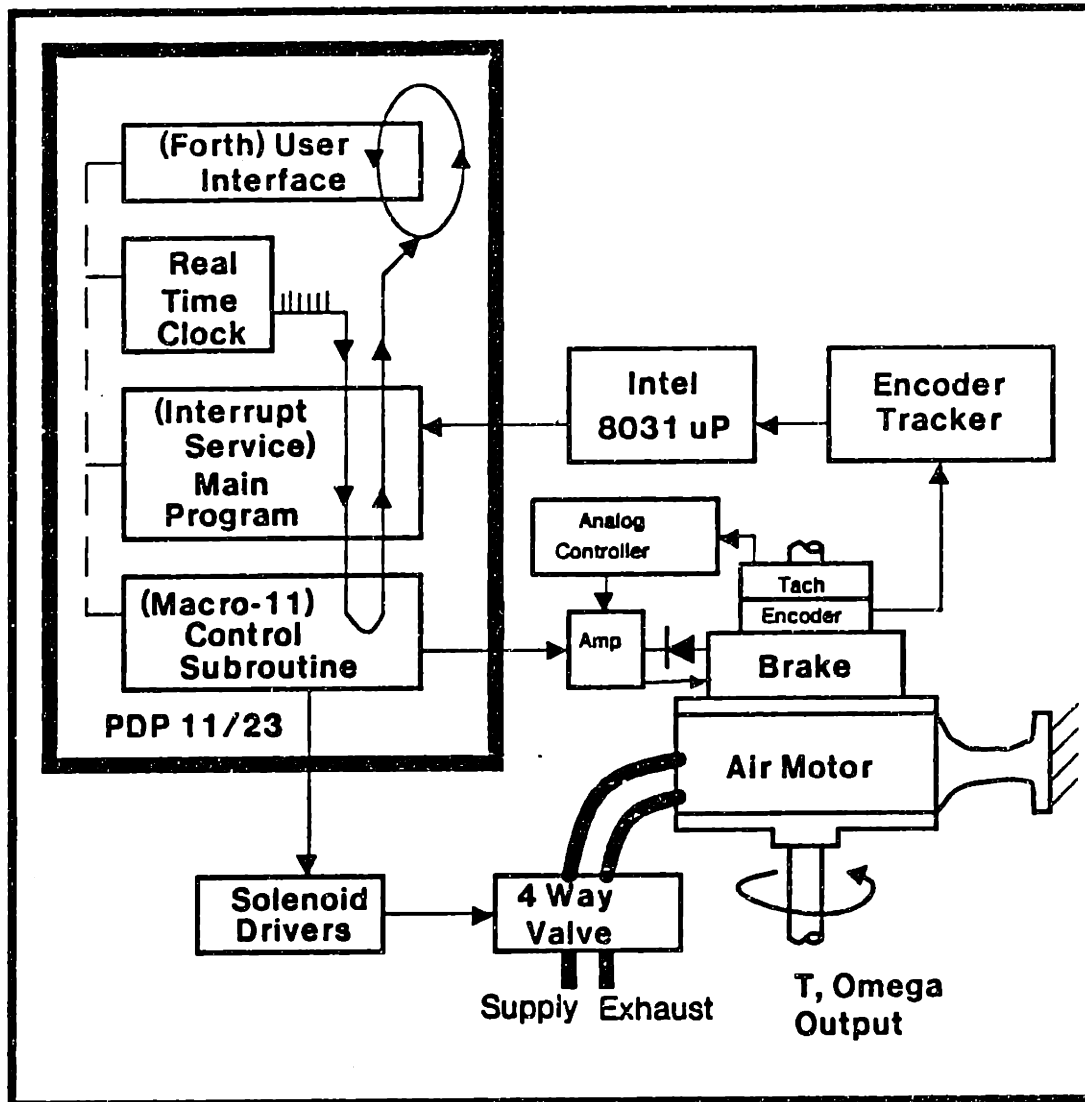
an encoder tracker. It was necessary to sample the tracker at 2Khz in order to avoid ambiguity in the count when the 8 bit counter rolled over. The main control program gathers position data at 500Hz from the Intel 8031 micro processor and passes it to the axis controller subroutine. The result of this process is a sampled sampled-data system. This would have given the same result as simply sampling the original signal at 500Hz if the 2 computers were perfectly synchronized.

Unfortunately, each processor was clocking off of a different clock, and hence the main control program, as it sampled the microprocessor count, had no guarantee of the uniformity in the number of μP sampling intervals represented. The end result is the same as sampling an analog signal which has the original position frequency content plus those required to make a 2Khz staircase. Since we were sampling at 500Hz the effects of aliasing were present and manifested themselves as a glitch every 25 or so samples.

The problem was resolved by synchronizing the 2 machines. They were synchronized by making the μP responsible for generating the control routine interrupt instead of the real-time clock in the PDP11.

The controller subroutine enables the appropriate solenoid driver, computes the difference equations, takes data, sends a control signal to the output amplifier and then returns to the main control program. If there are no more axes to run, the main program does a return from interrupt thus returning control to the FORTH user interface. The FORTH user interface is a relatively standard version of FORTH with linkage (indicated by the dashed lines) to the real-time clock, the control programs, and (not shown) to the Intel 8031, the amplifier, and the solenoid drivers. This linkage enables controller gains and position data to be accessed directly by the user.

6.1. Controller Subroutine

Figure 43 shows an expansion of the macro-11 control subroutine of Figure 42; the macro-11 code for this routine is given in appendix(iii).

Note that the sign of the proportional gain changes depending upon the direction of motion of the device. This is to compensate for the dependence of brake torque on direction of rotation. Also, if the position error is less than some allowable maximum the device enters a position holding mode (air pressure is switched off

66

Figure 43. Expansion of Macro 11 Control Subroutine

Take Data

New Set > Old Set
New Set < Old Set
New Set = Old Set

Gain = |Gain|
Solout = Backward

Gain = -|Gain|
Solout = Foreward

Error < Maxerr
Error > = Maxerr

Compute Difference Eqs
Linearization ?
Hysteresis Compensation ?

Solout = Off
Output = Vhold

Control Signal < 0
Control Signal > = 0

Amp Output = Negative

Amp Output = Positive

|Control Signal| > Vmax
|Control Signal| < = Vmax

Output = Control Signal

Output = Vmax ·

Send Output to Amplifier
Send Solout to Solenoids

Return from Subroutine

and a voltage corresponding to a holding torque is applied to the brake).

67

Figure 44. Experimental Step Response
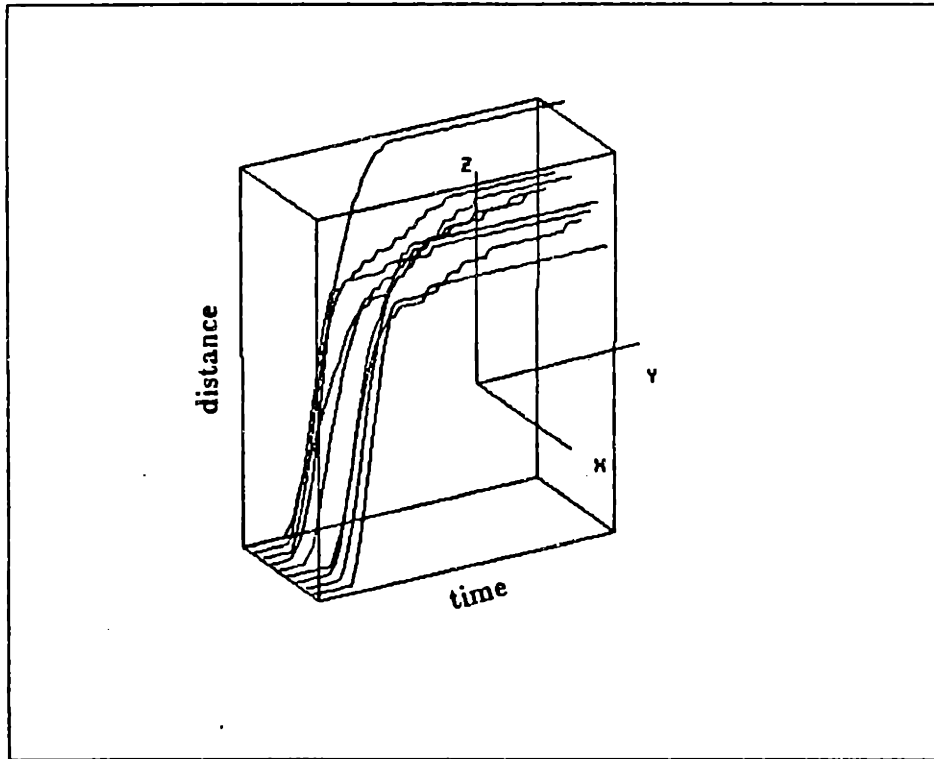
6.2. Experimental results

Actual Attainable Performance

A series of 9 experiments was performed for a step setpoint input of 50 encoder counts. Figure 44 shows the system response for each trial. The Y-axis corresponds to a time scale from 0 to 0.26 *sec*; the Z-axis to encoder position from 0 to 50 encoder counts; and the X-axis corresponds to experiment number.

A second series of text results is presented in Figure 45. Input conditions were the same as for those presented in Figure 44, but the brake offset torque was decreased slightly. Note that this parameter variation has a substantial effect on the response. The effect of this parameter could be thought of as resulting from a disturbing torque. This is unfortunate because the prototype actuator has a lot of intrinsic distrurbance torques. One of these is the static versus kinetic friction

Figure 45. Experimental Step Response
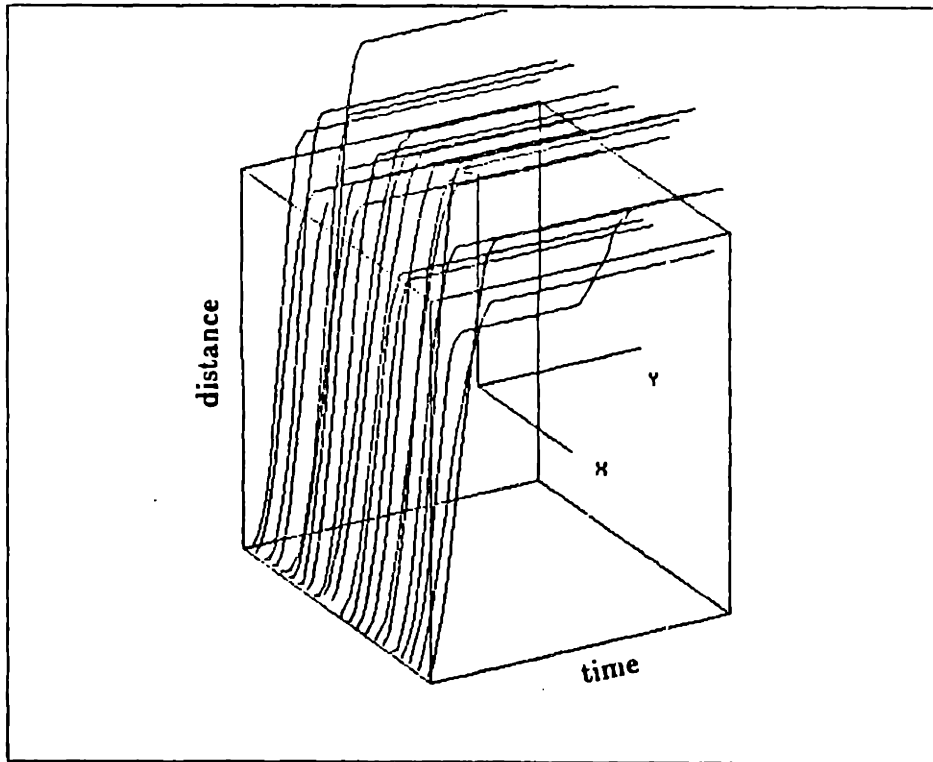
coefficients of the brake. Another is the stick-slip friction on the air motor vanes. Additionally, the MIT Cartesian Assembly Robot has a large amount of stiction.

As can be seen in Figures 44and 45 the steady state error of the actuator system is on the order of 10 encoder counts. This corresponds to a rotation of the actuator of 10/4000 of a revolution or 0.9 degrees. This repeatibility would be improved if the loop gain could be increased. Unfortunately, the present configuration severely limits the dynamic range of operation. The signal can saturate at several places around the control loop. The D/A range is only eight bits, and the maximum amplifier voltage in only 15 volts.

Figure 46 shows pairs of step responses for a variety of step sizes. The first pair corresponds to a step of 50 encoder counts, the second pair to 100 encoder counts, the third pair to 200 encoder counts, etc. The z-axis is normalized to the

Figure 46. Experimental Response to Large Steps
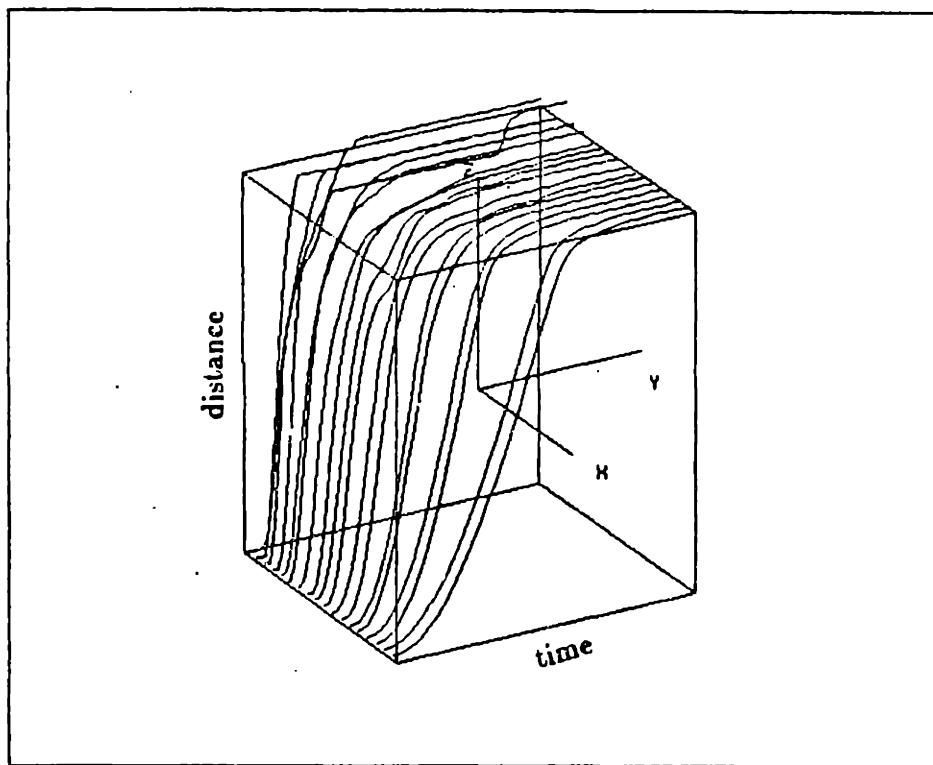
step size. Notice that the steady state error does not scale up with step size. Thus it can be assumed that the disturbance torques mentioned earlier, which do not vary with step size, are largely responsible for this steady state position error.

7. Conclusions

In its present configuration this device could be used for incremental motion applications where most of the moves are in the same direction. It would also be useful for devices that must rigidly hold their position. It is not good for continuous medium velocity applications as a large amount of power would be dissipated by the brake resulting in low efficiency and possible overheating. The system is good for high torque, low velocity operation where traditional DC motors have a very low efficiency.

7.1. Suggestions for Further Research and Improvements

Brake Modifications

The particle brake could be redesigned such that the torque/current curve is more linear, and hysteresis is reduced. This is especially important in the dynamic response. The electromagnetic design of the brake should be modified to a configuration in which it would respond more like an ideal inductor. This would probably involve a reduction of interwinding capacitance and choosing a core material with a linear response and minimum losses. Also, reduction of the inductive time constant would ease the control system requirements.

If this device is to be used in an industrial setting, a fail safe design which locked micro processor during power failures would be desirable. One possible way to accomplish this would be to incorporate a permanent magnet such that power must be supplied to obtain a zero torque output.

When this device is used for two successive moves in opposite directions there is a dwell time after the first move to allow for the solenoid valve to switch and air pressure to build micro processor in the opposite direction. This dwell time could be reduced or eliminated by a smart control algorithm which anticipated the correct switch time. A solution to this problem would find useful application in solenoid controlled air cylinders.

The air motor used in this prototype is constructed from cast iron and weighs 8 lbs. The weight of the device could be reduced to about 1/3 of its present weight by constructing it out of a lighter material such as aluminum. Additionally, unused material could be removed from the casting. The switch to a lighter material would also reduce the rotor inertia. This could be reduced even further by a redesign of the rotor.

The present system configuration uses a voltage amplifier to drive the particle brake. Ideally this results in a first order response of brake current to input voltage with the time constant being determined by the L_{brake}/R_{brake} of the brake coil winding. This first order response in addition to the 2nd order response of the inertial load results in a third order system. If a series resistor was added to the brake circuit and the output voltage of the amplifier was increased accordingly, the new time constant $(L_{brake}/(R_{brake} + R_{series}))$ might be small enough so that the system behaved as if it were second order thus simplifying the control algorithm. There are two main drawbacks to this. The first is that high voltage amplifiers are hard to find, expensive, and dangerous. The second is that it is likely that the added resistor will consume more power than the brake itself. A better solution would to use a current amplifier with a sufficiently high bus voltage to overcome the coil inductance.

In the present device the air power is not being used as effectively as possible. In particular the brake torque is fighting the air motor torque. Using an air servo valve would make the two devices more complimentary, however air servo valves are not cheap; on the order of $1000. If a cheap air servo valve is developed this would be attractive. In addition to complementing the brake the servo valve would substantially reduce the turn-around time-lag. This would raise the question of how to control an unusual two input single output system. Another alternative to the air servo valve would be a very fast air solenoid valve which could be pulse

width modulated. Some relatively fast solenoid valves do exist (5ms response time) however they are too small for this application. A response time on the order of fractions of a ms with an extremely high cycle life and high flow rate would be necessary.

An alternative hybrid actuator would be a DC motor coupled to a servoable brake. This would allow for extremely high deceleration rates and practically infinite stiffness for position holding. This arrangement would also raise the 2 input single output control question.

An alternative to reversing the air pressure to change directions is to use a reversing transmission. If one had a transmission capable of shifting in say $1ms$, the reversing could take place just as the actuator came to a halt. Since air pressure could be maintained during this time, full torque would be immediately available for acceleration in the opposite direction.

If the pressure in the input ports of the air motor was monitored, the solenoid valve could be switched before the device had reached its destination without confusing the controller. This would allow shorter turn around times, more efficient use of the air, and higher decellerations.

Since this device is sensitive to disturbing torques, it would be desirable to have a controller which rejected such disturbances. A no overshoot controller capable of doing this would be a Phelan controller applied to a third order system. This would result in a overall system of fourth order.

It would be interesting to do a general fourth order system analysis similar to the one in Chapter 5. Additionally the constraint of no velocity reversal could be made stronger by specifying that there be no "wiggle" in the position response. This condition stated mathematically is that there should be only three times during the response when the acceleration is equal to zero. These are at $t = 0$, $t = \infty$ and

one zero crossing somewhere inbetween.

8. Appendices

i. Error Analysis in Difference Equation Approximation

As can be seen in Figure 26 there are first and second derivatives taken in the feedback path. It is proposed to implement these derivatives as a first and second difference of the position signal. A rule of thumb when using the backward rectangular rule for approximating first derivatives is to have the sampling frequency 10 times higher than the highest frequency being sampled.

Velocity Errors from Difference Equation

The following analysis will relate the errors incurred using a second difference backward rectangular approximation to those of a first difference.

Given a the following signal to be sampled

$$x = \sin(\omega t) \tag{i1}$$

which is sampled at times τ and has first exact derivative

$$\omega \cos(\omega t) \tag{i2}$$

The first difference using the backward rectangular rule is

$$\frac{x(t) - x(t - \tau)}{\tau} \tag{i3}$$

A normalized velocity error in this approximation can be defined as follows

$$E_{vel}(\tau, \omega, t) = \frac{\dot{x}_{exact} - \dot{x}_{approx}}{\omega} \tag{i4}$$

Performing a trigonometric expansion and factoring yields this expression for the error.

$$E_{vel}(\tau, \omega, t) = C(\omega, \tau)\cos(\omega t) + D(\omega, \tau)\sin(\omega t) = E_{vel}^0 \sin(\omega t + \phi_{vel}(\tau, \omega)) \quad (i5)$$

where

$$C = \frac{-\sin(\omega\tau) - \omega\tau}{\omega\tau} \quad (i6)$$

$$D = \frac{\cos(\omega\tau) - 1}{\omega\tau} \quad (i7)$$

$$E_{vel}^0 = \sqrt{C^2 + D^2} \quad (i8)$$

$$\phi_{vel} = \tan^{-1}(\frac{C}{D}) \quad (i9)$$

Acceleration Errors from Difference Equation

Taking the second derivative of the original signal yields

$$-\omega^2 \sin \omega t \quad (i10)$$

The second difference approximation to this, again using the backward rectangular rule, is

$$\frac{x(t) - 2x(t - \tau) + x(t - 2\tau)}{\tau^2} \quad (i11)$$

A normalized acceleration error in the approximation can be defined as follows.

$$E_{acc}(\tau, \omega, t) = \frac{\ddot{x}_{exact} - \ddot{x}_{approx}}{\omega^2} \qquad (i12)$$

Substituting for x, doing a trigonometric expansion, and factoring yields the following formulation for the error.

$$E_{acc}(\tau, \omega, t) = F(\omega, \tau)\cos(\omega t) + G(\omega, \tau)\sin(\omega t) = E^0_{acc}\sin(\omega t + \phi_{acc}(\omega, \tau)) \qquad (i13)$$

Where

$$F = \frac{\sin(2\omega\tau) - 2\sin(\omega\tau)}{\tau^2\omega^2} \qquad (i14)$$

$$G = \frac{-\cos(2\omega\tau) + 2\cos(\omega\tau) - 1}{\omega^2\tau^2} \qquad (i15)$$

$$E^0_{acc} = \sqrt{F^2 + G^2} \qquad (i16)$$

$$\phi_{acc} = \tan^{-1}\left(\frac{F}{G}\right) \qquad (i17)$$

The parameters $E^0_{vel}, E^0_{acc}, \phi_{vel}, \phi_{acc}$ are plotted in Figure 47 for $\omega = 2\pi$ and $0 \leq \tau \leq 0.5$ Notice that for $\tau = 0.05$ the magnitude of the acceleration error is approximately equal to that of the velocity error when $\tau = 0.1$ which maps the rule of thumb mentioned earlier to the case of the second difference.

Therefore the sample frequency should be 20 times the frequency of the highest sampled frequency for a "reasonable" second difference derivative approximation.

Figure 47. Errors from First and Second Backward Diff Approx
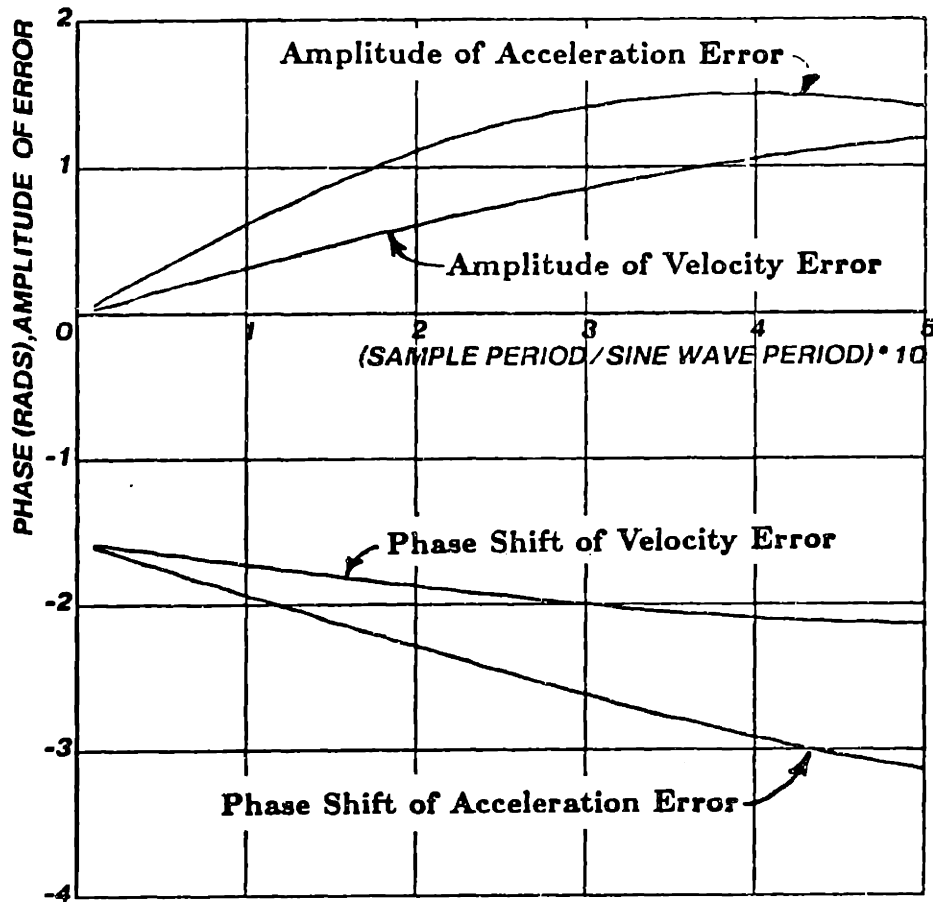
ii. Matching Model State Feedback with Difference Equations

In order to implement the feedback transfer function

$$1 + K_v s + K_a s^2 \qquad (ii1)$$

the backward rectangular Z transform is

$$s = \frac{1 - z}{\tau z} \qquad (ii2)$$

where τ is the sample period was used. This results in the following difference equation in the position variable X.

$$\frac{(\tau^2 + K_v\tau + K_a)X_n - (K_v\tau + 2K_a)X_{n-1} + K_aX_{n-2}}{\tau^2} \qquad (ii3)$$

iii. Macro 11 Control Program

```
        AC0 = %0            ; Assign symbols to
        AC1 = %1            ; FPP accumulators
        AC2 = %2
        AC3 = %3


        DTOA  = 167773      ; 1 Byte digital to analog output


        .EVEN
DMAX:  .FLT2  255.0         ; Max D/A output for comparison
DMIN:  .FLT2  0.0           ; Min D/A output for comparison
DMAXI: .WORD  255.          ; Max D/A output for output
DMINI: .WORD  0             ; Min D/A output for output
OUT:   .WORD  0             ; Temp output variable


X1:    .FLT2  0.0           ; Position delayed 1 sample
X2:    .FLT2  0.0           ; Position delayed 2 samples
BIAS:  .FLT2  128.0         ; Make D/A offset 128


YG::   .FLT2  1.0           ; Proportional gain
G0:    .FLT2  1.0           ; Feedback Diff Eq Coefficients
G1:    .FLT2  0.0           ; G0*X0 - G1*X1 + G2*X2
G2:    .FLT2  0.0


POINT: .WORD  DATA + 1024.  ; Pointer initialized to end of data
DATA:  .BLKW  512.          ; Buffer for position data



YAXIS:: CMP    # DATA + 1024.,POINT   ; Pointer outside of buffer ?
        BLE    FULL         ; Yes - Have enough data
        LDF    @R1,AC0      ; Convert to integer
        STCFI  AC0,@POINT   ; Save data
        ADD    # 2,POINT    ; Increment pointer



FULL:  LDF    G0,AC0        ; Compute insividual feedback terms
       MULF   @R1,AC0

       LDF    G1,AC1
       MULF   X1,AC1
```

```
        LDF     G2,AC2
        MULF    X2,AC2

        SUBF    AC1,AC0         ; Sum terms
        ADDF    AC2,AC0         ; AC0 = G0*X0 - G1*X1 + G2*X2

        LDF     AC0,AC1         ; AC1 = Position feedback term
        LDF     @R2,AC0         ; AC0 = Set Point
        SUBF    AC1,AC0
        MULF    YG,AC0          ; AC0 = Control signal
        ADDF    BIAS,AC0        ; Make D/A output offset BIAS

CONT:   CMPF    DMAX,AC0        ; Compare output to DMAX
        CFCC
        BMI     MXOUT           ; Jump if positive saturation

        CMPF    DMIN,AC0        ; Compare output to DMIN
        CFCC
        BPL     MNOUT           ; Jump if negative saturation

        STCFI   AC0,OUT         ; No clipping
        JMP     DONE

MXOUT:  MOV     DMAXI,OUT
        JMP     DONE

MNOUT:  MOV     DMINI,OUT
        JMP     DONE

DONE:   MOVB    OUT,DTOA        ; Talk to real world

        LDF     X1,AC0          ; Save old position samples
        STF     AC0,X2

        LDF     @R1,AC0
        STF     AC0,X1

        RTS     PC              ; Go back to main program
        .END
```

9. References

1. Seering, W. P., "Directions in Robot Design," Journal of Mechanisms, Transmissions, and Automation in Design, Vol. 1, April 1983.

2. Pieper, D. L., "The Kinematics of Manipulators Under Computer Control," Proceedings of the 2nd International Congress on the Theory of Machines and Mechanisms, Vol. 2, 1969, pp. 159-168.

3. Roth, B., "Performance Evaluation of Manipulators from a Kinematic Viewpoint," Performance Evaluation of programmable Robots and Manipulators, National Bureau of Standards Special Publication 459, pp. 39-62.

4. Yang, D.C.H., and Lee, T. W., "On the Workspace of Mechanical Manipulators," Journal of Mechanisms, Transmissions, and Automation in Design, Vol. 1, April 1983.

5. Tsai, Y. C., and Soni, A. H., "An Algorithm for the Workspace of a General n-R Robot," Journal of Mechanisms, Transmissions, and Automation in Design, Vol. 1, April 1983.

6. Paul, R. P., "Robot Manipulators: Mathematics, Programming and Control," The M.I.T. Press, Cambridge, MA, 1981.

7. Vukobratovic, M., and Kircanski, M., "One Method for Optimal Synthesis of Manipulation Robot Trajectories," Journal of Dynamic Systems, Measurement, and Control, ASME, Vol. 104, pp. 188-193, June 1982.

8. Hollerbach, J., "An Iterative Lagrangian Formulation of Manipulator Dynamics," M.I.T. Artificial Intelligence Laboratory A.I. Memo No. 533, Cambridge, MA, April 1980.

9. Book, W. J., "Analysis of Massless Elastic Chains with Servo Controlled Joints," ASME Journal of Dynamic Systems, Measurement and Control, vol. 101,

pp. 187-192, 1979.

10. Book, W. J., Maizza-Neto, O., and Whitney, D. E., "Feedback Control of Two Beam, Two Joint Systems with Distributed Flexibility," ASME Journal of Dynamic Systems, Measurement, and Control, pp. 424-431, December 1975.

11. Sunada, W., and Dubowsky, S., "On the Dynamic Analysis and Behavior of Industrial Robotic Manipulators with Elastic Members," Journal of Mechanisms, Transmissions, and Automation in Design, Vol. 1, April 1983.

12. Phelan, R.M., "A Simplified Approach to Feedback Control System Design," ASME Design Engineering Conferences, Anaheim 1978, Chicago 1979.

13. Hune, G., "Drive, Particularly for an Industrial Manipulator," United States Patent 4,339,984, July 20, 1982.

14. Bass, G.A., "Modeling and Control of a Hydro-Pneumatic Actuator," Thesis, Master of Science, University of California, Davis, 1980.

15. Ogata, K., "Modern Control Engineering," Prnetice-Hall, Inc., Englewood Cliffs, N.J., 1970.

16. Oppenheim, A.V., Schafer, R.W., "Digital Signal Processing," Prentice -Hall, Inc., Englewood Cliffs, N.J., 1975.

17. Meyfarth, P.F., "Dynamic Response Plots and Design Charts for Third-Order Linear Systems", MIT Dynamic Anslysis and Control Laboratory Dept. of Mech. Eng. Research Memo. No. 7401-3, 19 58